

Sensor and Simulation Notes

Note 185

September 1973

Transmission Line Model of Radiating Dipole
with Special Form of Impedance Loading

David L. Wright
James F. Prewitt
The Dikewood Corporation
Albuquerque, New Mexico 87106

CLEARED
FOR PUBLIC RELEASE
PL/PA 16 DEC 96

Abstract

This note considers the far-field radiated waveform and field pattern from a long, thin, cylindrical antenna in the transmission line approximation when driven by a voltage generator of waveform $V_0 u(t)$ where $u(t)$ is the unit step function. The antenna is loaded with an impedance which is taken to have the form

$$Z' = \frac{2Z_\infty \delta(\omega)}{h - \zeta}$$

where h is the antenna half-length, ζ is the absolute value of the distance measured along the antenna from the center, Z_∞ is an approximate antenna characteristic impedance based on that of a long, thin biconical antenna, and $\delta(\omega)$ is a complex function of frequency. Analytical and numerical solutions for the far field pattern and waveform are discussed. In particular, the effects of resistive with parallel inductive loading are discussed.

PL 96-0938

Sensor and Simulation Notes

Note 185

September 1973

Transmission Line Model of Radiating Dipole
with Special Form of Impedance Loading

David L. Wright
James F. Prewitt
The Dikewood Corporation
Albuquerque, New Mexico 87106

Abstract

This note considers the far-field radiated waveform and field pattern from a long, thin, cylindrical antenna in the transmission line approximation when driven by a voltage generator of waveform $V_0 u(t)$ where $u(t)$ is the unit step function. The antenna is loaded with an impedance which is taken to have the form

$$Z' = \frac{2Z_\infty \delta(\omega)}{h - \zeta}$$

where h is the antenna half-length, ζ is the absolute value of the distance measured along the antenna from the center, Z_∞ is an approximate antenna characteristic impedance based on that of a long, thin biconical antenna, and $\delta(\omega)$ is a complex function of frequency. Analytical and numerical solutions for the far field pattern and waveform are discussed. In particular, the effects of resistive with parallel inductive loading are discussed.

Acknowledgment

The authors would like to thank Dr. Carl E. Baum for his helpful suggestions and interest in this work.

I. Introduction

One of the problems of pulse radiating dipole antennas is that of selecting loading on the antenna in such a way as to optimize the radiated waveform in terms of some desired waveshape. This problem may be attacked in a number of ways. One example is the work of D. E. Mewether^{1, 2} in which a synthesis procedure is developed for selecting lumped resistor pairs to symmetrically load a cylindrical antenna so that the far zone electromagnetic field pulse or near zone magnetic field approximates some prescribed waveshape.

Another example is the work of C. E. Baum³ who considers continuously loaded axially and lengthwise symmetric pulse radiating dipoles using a transmission line approximation for finding the currents on the antenna. Baum considers first a uniformly resistively loaded case and then a special case of non-uniform loading. This special loading is proportional to $(h - |z|)^{-1}$ where h is the half length of the antenna and z is the position on the antenna measured from the center (driving point). This form of resistive loading has been previously considered by Wu and King⁴ and Shen and Wu⁵ from the standpoint of frequency domain broadband and directional properties. The reason for the reappearance of this special form of resistive loading in pulse studies is the broadbanding property of this type of loading which permits pulse smoothing of a kind desirable in EMP waveform simulation.

The present study is largely an extension of the work of reference 3. The same functional form of loading is retained, but the proportionality is no longer fixed at a single value. Variation over real and complex values is permitted corresponding to physical variation over resistive and reactive values. Normalized current distributions and radiated electric fields are given in both frequency and time domain as a function of loading and observer angle with respect to the antenna.

II. Formulation and Solution of the Current Equation

The antenna geometry is shown in figure 1. As the first step in our analysis we require the antenna current. To obtain an approximation to the current we employ a transmission line model for the antenna. It has been shown^{3, 4} that in this zero-order or transmission line approximation the wave equation for the current on a thin dipole antenna may be written as

$$\frac{\partial^2 \tilde{I}}{\partial \xi^2} - (\gamma_0^2 + s C' Z') \tilde{I} = 0 \quad (1)$$

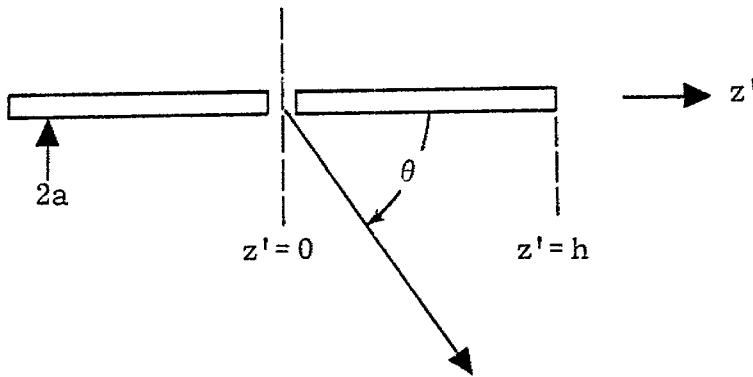


Figure 1. Geometry of the Problem

where s is the Laplace variable,

$$\gamma_0 = \frac{s}{c}$$

$$C' = \frac{1}{cZ_{\infty}} \quad \text{equivalent transmission line capacitance per unit length}$$

Z' = equivalent transmission line loading per unit length

$$Z_{\infty} \approx \frac{Z_0}{\pi} \ln \left(\frac{2h}{a} \right) \quad h \gg a \quad \text{characteristic impedance of long, thin biconical antenna exclusive of loading} \quad (2)$$

a = antenna radius

$2h$ = antenna length

$$Z_0 = \sqrt{\frac{\mu_0}{\epsilon_0}} \quad \text{impedance of free space}$$

$$\xi = |z'|$$

and the tilde indicates that we are in the Laplace or frequency domain.

At this point take

$$Z' = \frac{2Z_{\infty} \delta}{h-\xi} \quad (3)$$

where δ is in general a complex function of frequency, but is independent of ξ . Substituting for C' and Z' in equation 1, the wave equation for \tilde{I} becomes

$$\frac{\partial^2 \tilde{I}}{\partial \xi^2} - \left(\gamma_0^2 + \frac{2\gamma_0 \delta}{h-\xi} \right) \tilde{I} = 0 \quad (4)$$

If a trial solution for the current is written in the form

$$\tilde{I}(s, \xi) = (h - \xi) e^{-\gamma_0 \xi} \Phi(s, \xi) \quad (5)$$

and equation 5 substituted into equation 4 we find that $\Phi(s, \xi)$ satisfies the differential equation

$$(h-\xi) \frac{\partial^2 \Phi}{\partial \xi^2} - 2 \frac{\partial \Phi}{\partial \xi} \left[\gamma_0 (h-\xi) + 1 \right] + 2\gamma_0 (1-\delta) \Phi = 0 \quad (6)$$

Making a change of variable

$$y = -2\gamma_0 (h - \xi), \quad (7)$$

we obtain

$$y \frac{\partial^2 \Phi}{\partial y^2} + (2-y) \frac{\partial \Phi}{\partial y} + (\delta - 1) \Phi = 0. \quad (8)$$

This is the Kummer or confluent hypergeometric equation as given, for example, by equation 13.1.1 of Abramowitz and Stegun.⁶

This differential equation has a solution of the form

$$\Phi(y) = C_1 M(1 - \delta, 2; y) + C_2 U(1 - \delta, 2; y) \quad (9)$$

where M and U are Kummer's confluent hypergeometric functions.

Thus, a general solution for the current is

$$\tilde{I}(s, \xi) = (h-\xi) e^{-\gamma_0 \xi} \left\{ C_1 M \left[1-\delta, 2; -2\gamma_0 (h-\xi) \right] + C_2 U \left[1-\delta, 2; -2\gamma_0 (h-\xi) \right] \right\}. \quad (10)$$

Requiring the current to vanish at the ends of the antenna, so that $\tilde{I}(s, h) = 0$, we must set $C_2 = 0$ since

$$U(a, 2; z) \sim O\left(\frac{1}{z}\right) \text{ as } z \rightarrow 0$$

and

$$M(a, 2; 0) = 1.$$

Therefore

$$\tilde{I}(s, \xi) = (h - \xi) e^{-\gamma_0 \xi} C_1 M \left[1 - \delta, 2; -2\gamma_0(h - \xi) \right] \quad (11)$$

Writing C_1 in terms of the current at the center of the antenna

$$C_1 = \frac{\tilde{I}(s, 0)}{hM(1 - \delta, 2; -2\gamma_0 h)} \quad (12)$$

so that

$$\tilde{I}(s, \xi) = (1 - \xi/h) e^{-\gamma_0 \xi} \tilde{I}(s, 0) \frac{M \left[1 - \delta, 2; -2\gamma_0(h - \xi) \right]}{M(1 - \delta, 2; -2\gamma_0 h)} \quad (13)$$

To evaluate the driving point current we continue to use the transmission line approximation. From one of the transmission line equations we may write

$$\tilde{V}(s, \xi) = -\frac{1}{sC'} \frac{\partial \tilde{I}}{\partial \xi} \quad (14)$$

Substituting the expression for $\tilde{I}(s, \xi)$ of equation 13 into equation 14

$$\tilde{V}(s, \xi) = \frac{\left[\gamma_0(h - \xi) + 1 \right] M \left[-2\gamma_0(h - \xi) \right] - 2\gamma_0(h - \xi) M' \left[-2\gamma_0(h - \xi) \right]}{sC'h M(-2\gamma_0 h)} \tilde{I}(s, 0) e^{-\gamma_0 \xi} \quad (15)$$

The voltage at the center of the antenna can then be written

$$\tilde{V}(s, 0) = \frac{1}{sC'h} \frac{(\gamma_0 h + 1) M(-2\gamma_0 h) - 2\gamma_0 h M'(-2\gamma_0 h)}{M(-2\gamma_0 h)} \tilde{I}(s, 0) \quad (16)$$

Here for simplicity we have written $M(a, b; z)$ as $M(z)$ and $\frac{\partial M(a, b; z)}{\partial z}$ as $M'(z)$

Then the antenna impedance in the transmission line approximation is

$$\begin{aligned} Z_a &= \frac{\tilde{V}(s, 0)}{\tilde{I}(s, 0)} = \frac{1}{sC'h} \frac{(\gamma_0 h + 1) M(-2\gamma_0 h) - 2\gamma_0 h M'(-2\gamma_0 h)}{M(-2\gamma_0 h)} \\ &= \frac{1}{sC'h} \left[(\gamma_0 h + 1) - 2\gamma_0 h \frac{M'(-2\gamma_0 h)}{M(-2\gamma_0 h)} \right] \end{aligned} \quad (17)$$

Defining

$$f_\delta = 2 \frac{M'(-2\gamma_0 h)}{M(-2\gamma_0 h)} \quad (18)$$

and remembering that $\gamma_0 = \frac{s}{c}$ and $C' = \frac{1}{cZ_\infty}$, we have finally

$$Z_a = Z_\infty \left[\frac{1}{s_h} + 1 - f_\delta \right] \quad (19)$$

where $s_h \equiv \frac{sh}{c}$.

Thus equation 13 may be written in terms of $\tilde{V}(s, 0)$ as

$$\tilde{I}(s, \xi) = \frac{\tilde{V}(s, 0)(1-\xi/h) e^{-\gamma_0 \xi} M[1-\delta, 2; -2\gamma_0(h-\xi)]}{Z_\infty \left[\frac{1}{s_h} + 1 - f_\delta \right] M[1-\delta, 2; -2\gamma_0 h]} \quad (20)$$

Equation 20 is then the solution for the frequency domain current on the antenna for an arbitrary driving function $\tilde{V}(s)$ in the transmission line approximation and with no special treatment for the feedpoint geometry.

III. Current Solution for Step Function Input

Equation 20 gives the solution for the frequency domain current for an arbitrary driving function. At this point we specialize to the case where the antenna is driven by an idealized capacitive pulse generator of capacitance C_g , impedance $Z_g = \frac{1}{sC_g}$, and voltage output $\tilde{V}_g(s) = \frac{V_o}{s}$. Schematically, the situation is shown in Figure 2. Note that the generator

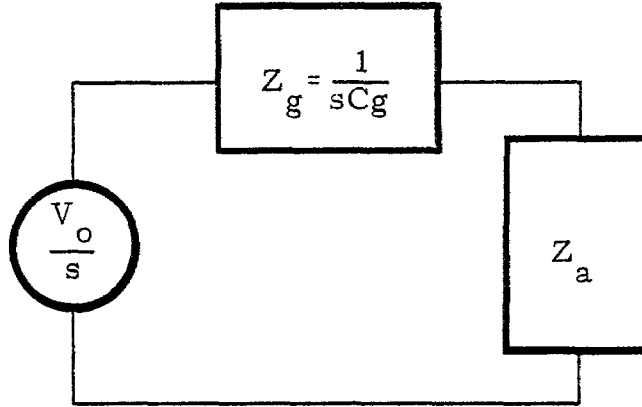


Figure 2

Schematic Representation of Capacitive Generator
Driving Antenna

impedance appears in series with that of the antenna and that therefore $\tilde{V}_g(s)$ is not identical to $\tilde{V}(s, 0)$. From the circuit of Figure 2, however, we may write

$$\tilde{I}(s, 0) = \frac{V_o}{s} \left[Z_g + Z_a \right]^{-1} \quad (21)$$

Substituting for Z_a from equation 19 into equation 21 we obtain

$$\tilde{I}(s, 0) = \frac{V_o}{s} \left[\frac{1}{sC_g} + \frac{1}{sC_a} + Z_\infty - Z_\infty f_\delta \right]^{-1} \quad (22)$$

where $C_a = C'h$.

Define a parameter $\alpha \equiv 1 + \frac{C_a}{C_g}$. Equation 22 becomes

$$\tilde{I}(s, 0) = \frac{V_o}{sZ_\infty} \left[\frac{c\alpha}{s_h} + 1 - f_\delta \right]^{-1} \quad (23)$$

Substituting equation 23 into equation 13, we obtain

$$\tilde{I}(\xi) = \frac{V_o}{Z_\infty} \frac{h}{[\text{sh}(1-f_\delta) + c\alpha]} \left[1 - \frac{\xi}{h} \right] e^{-\frac{s\xi}{c}} \frac{M[1-\delta, 2; -2\gamma_o(h-\xi)]}{M(1-\delta, 2; -2\gamma_o h)} \quad (24)$$

Figures 3 through 9 show current distribution along the antenna. Each figure is for a discrete frequency, $\omega = ck$, and treats the loading, δ , as a parameter. Figures 3 and 4 include relative phase, $\arg[I(z')/I(0)]$. It may be observed that for any frequency both the magnitude and phase of the current are linear functions if δ is taken to be unity. This is not true for other values of loading. The curves in figures 3 through 9 are obtained from equation 24 with the results normalized to $\tilde{I}(0)$. It should be remembered, however, that $\tilde{I}(0)$ is a function of frequency. Therefore no comparison of absolute values of currents at different frequencies is to be made from the figures. This information is available only by first calculating $\tilde{I}(\delta, 0)$ for some particular $s = j\omega$ by using equation 23.

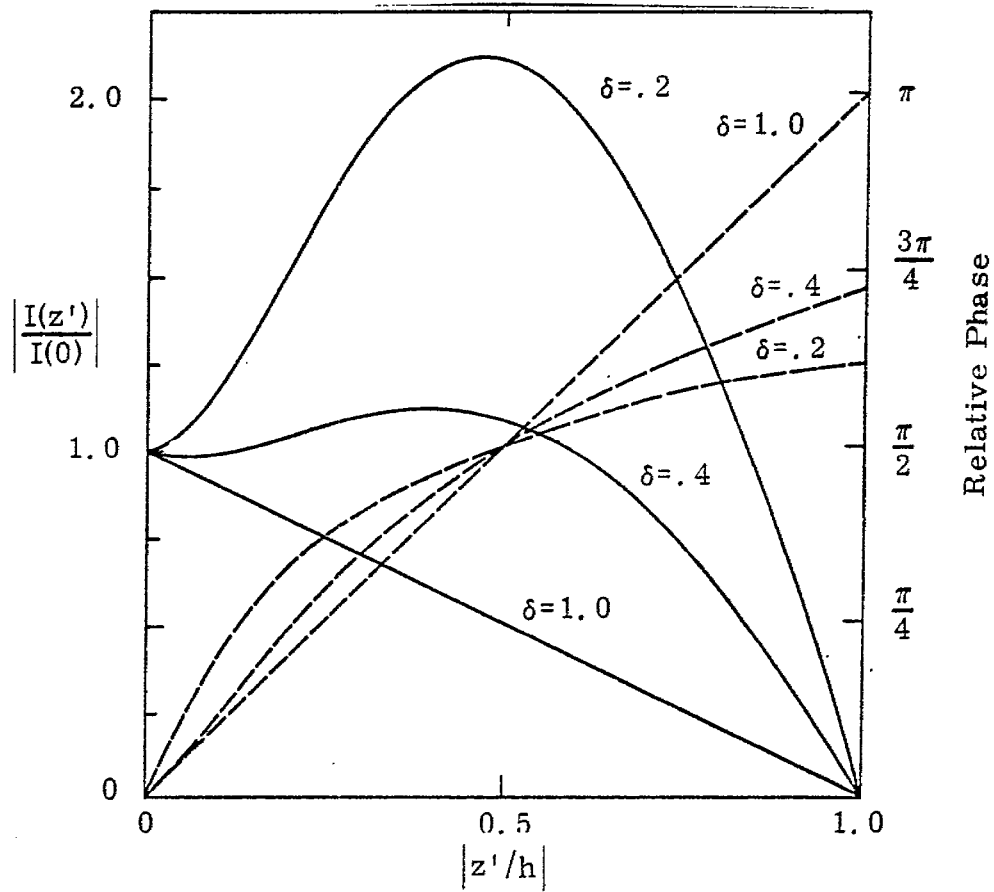


Figure 3. Normalized Current Distribution for $kh = \pi$ and $\delta = .2, .4, 1.0$

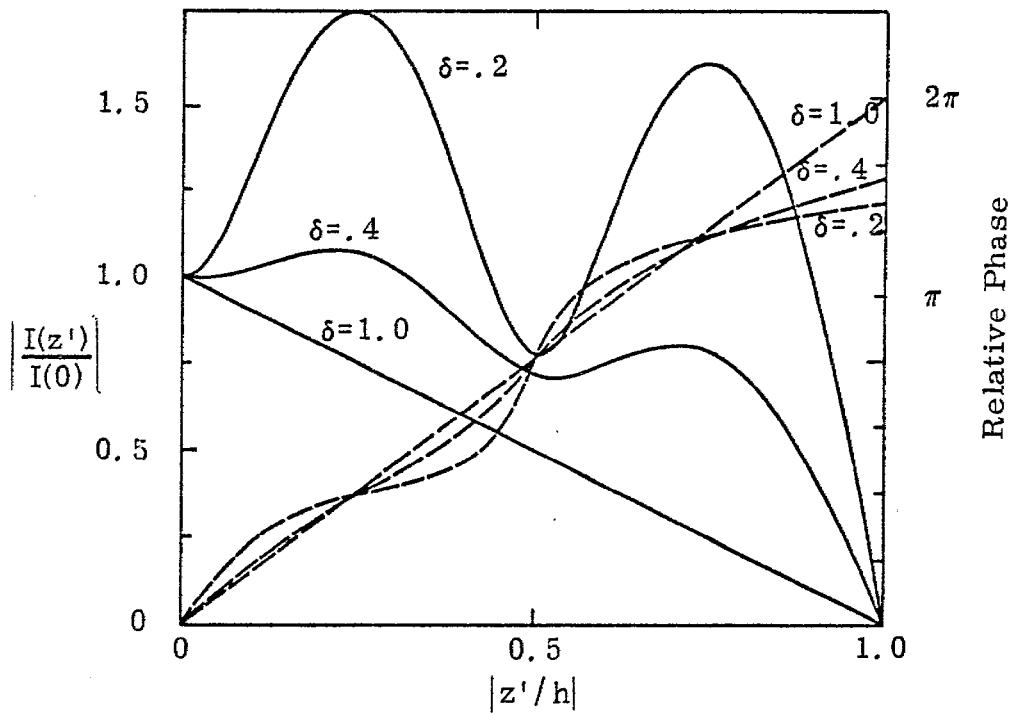


Figure 4. Normalized Current Distribution for $kh = 2\pi$, $\delta = .2, .4, 1.0$

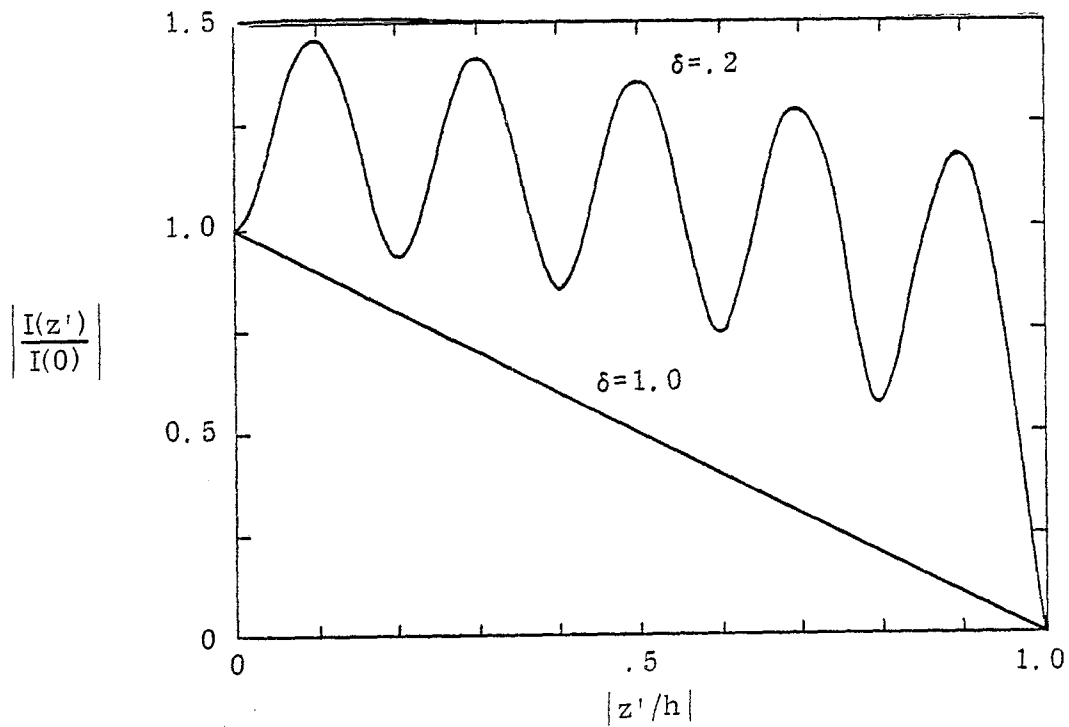


Figure 5. Magnitude of Normalized Current Distribution for $kh = 5\pi$ and $\delta = .2, 1.0$

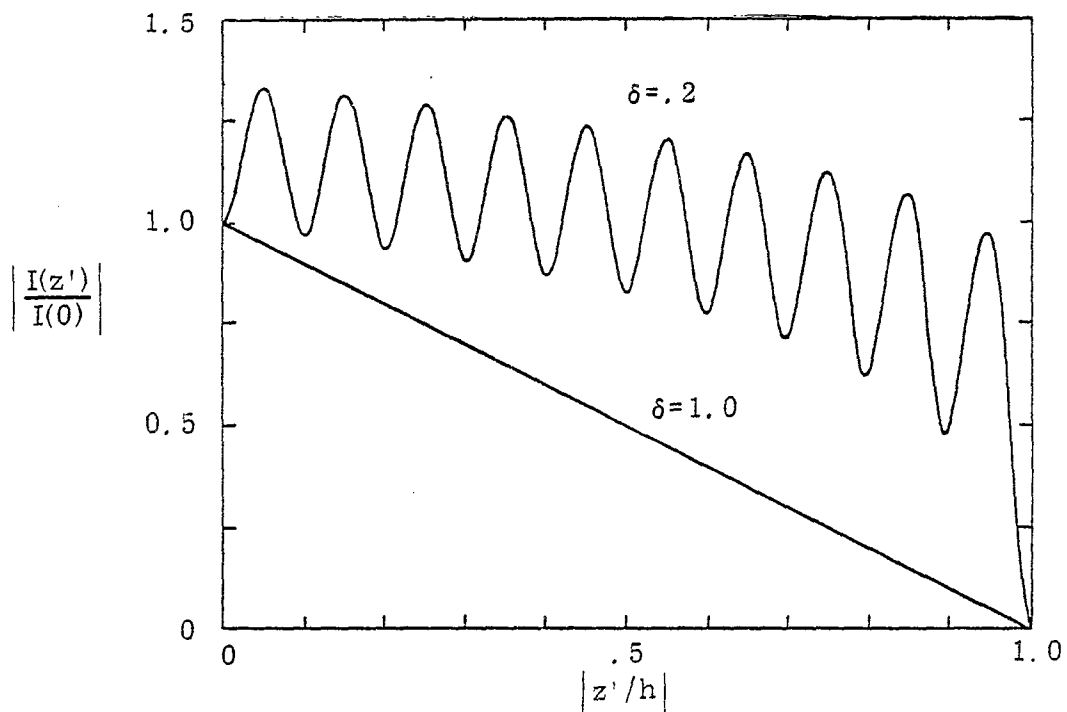


Figure 6. Magnitude of Normalized Current Distribution for $kh = 10\pi$ and $\delta = .2, 1.0$

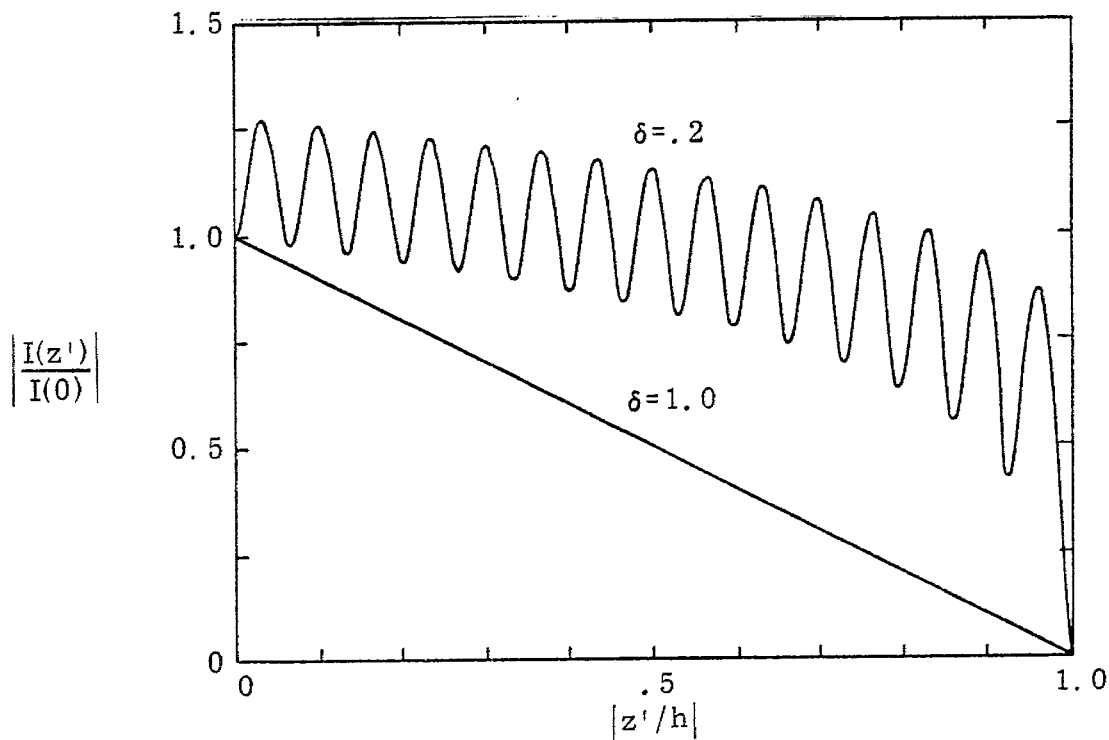


Figure 7. Magnitude of Current Distribution for $kh = 15\pi$ and $\delta = .2, 1.0$

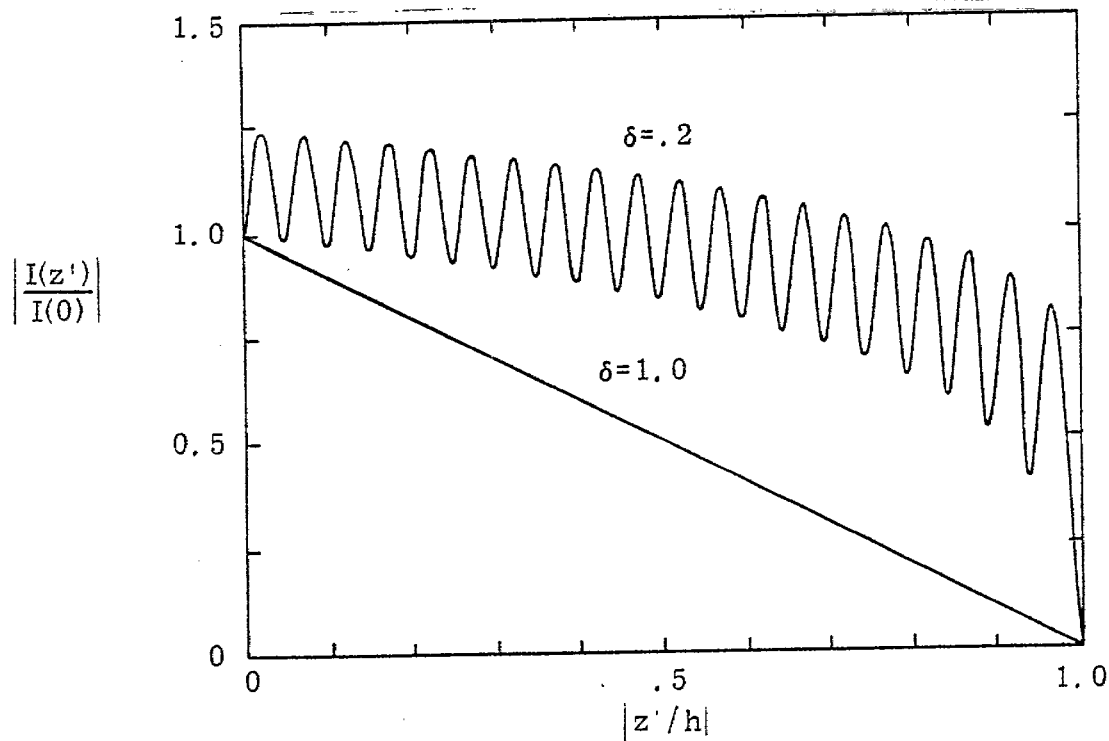


Figure 8. Magnitude of Normalized Current Distribution for $kh = 20\pi$ and $\delta = .2, 1.0$

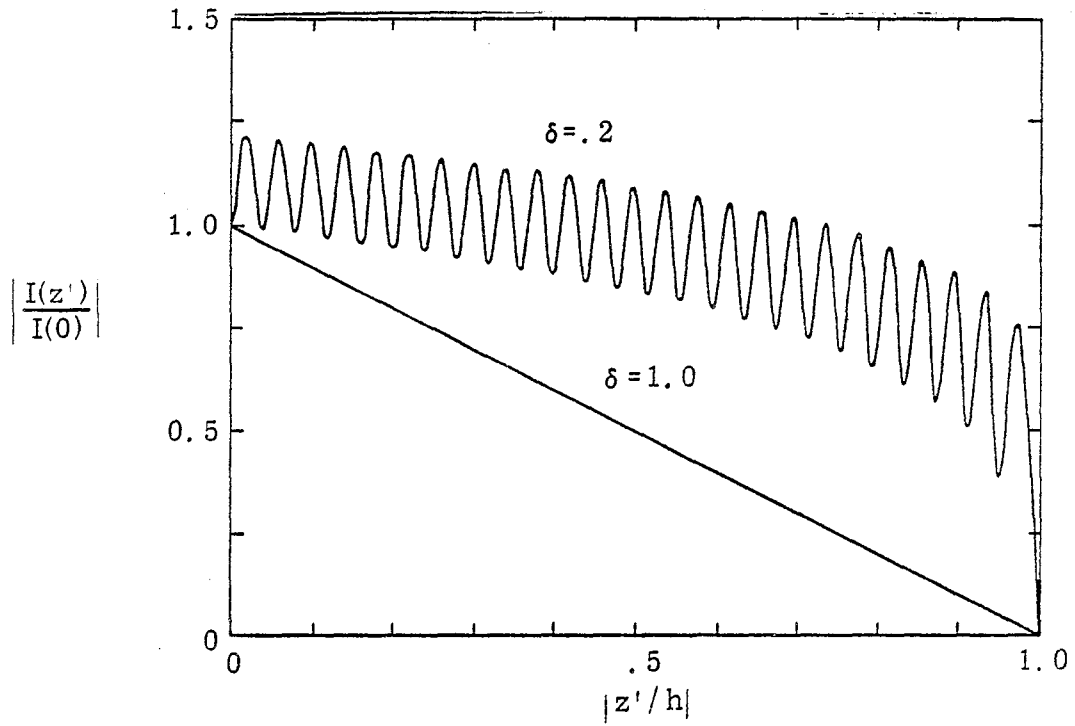


Figure 9. Magnitude of Normalized Current Distribution for $kh = 25\pi$ and $\delta = .2, 1.0$

IV. Radiated Field

Using a thin-wire approximation, we assume that I is concentrated on the z' axis. Following reference 3 the normalized radiated waveform is then calculated as

$$\tilde{\xi}(\theta) = \frac{\mu_0}{4\pi} \frac{s}{V_0} \int_{-h}^h \tilde{I}(z') e^{\gamma_0 z' \cos(\theta)} dz' \quad (25)$$

$$\xi(\theta) = \sin(\theta) \frac{\mu_0}{4\pi} \frac{1}{V_0} \frac{\partial}{\partial t} \int_{-h}^h I\left(z', t^* + \frac{z' \cos(\theta)}{c}\right) dz'$$

where t^* is the retarded time given by

$$t^* \equiv t - \frac{r}{c} \quad (26)$$

The normalized waveform in equation 25 is related to the far or radiated electric field $E_{f\theta}$ (only a θ component) by

$$\xi \equiv \frac{r E_{f\theta}}{V_0}, \text{ and } \tilde{\xi} \equiv \frac{r \tilde{E}_{f\theta}}{V_0} e^{\gamma_0 r} \quad (27)$$

In addition $\xi' \equiv 2\pi f_g \xi$, $\tilde{\xi}' \equiv 2\pi f_g \frac{\xi}{t_h}$

where $f_g \equiv \frac{Z_\infty}{Z_0}$, $t_h \equiv \frac{h}{c}$. Also define $\tau_h \equiv \frac{ct-r}{h}$. Note that ξ is considered using retarded time so that a current wave initiated at $t = 0$ at the center of the antenna will produce a waveform at the observer beginning at $t^* = 0$.

Substituting for $\tilde{I}(\xi)$ with $\xi = |z'|$ into the first of equations 25, and using equations 27 we obtain

$$\tilde{\xi}(\theta) = \frac{\sin\theta}{2} \frac{s}{[\text{sh}(1-f_\delta) + c\delta]} \frac{1}{M(-2\gamma_0 h)} \times \int_{-h}^h \left[1 - \frac{|z'|}{h} \right] M \left[-2\gamma_0 (h - |z'|) \right] e^{\frac{s}{c}(-|z'| + z' \cos \theta)} dz' \quad (28)$$

The inverse transform of the far field frequency domain result in equation 28 yields the time domain result. For certain cases analytic closed form inversions have been obtained. For other cases numerical inversions were carried out. Curves of magnitude and phase of $\tilde{\xi}'(\theta)$ as a function of frequency for various values of observer angle θ and loading δ are given in figures 10 through 15.

In figures 10 through 15 the patterns are for fixed frequencies with resistive loading as a parameter. All patterns are normalized to the maximum value, so that directionality as a function of loading is indicated, but in general, the peak value of E_θ is not the same for various values of δ .

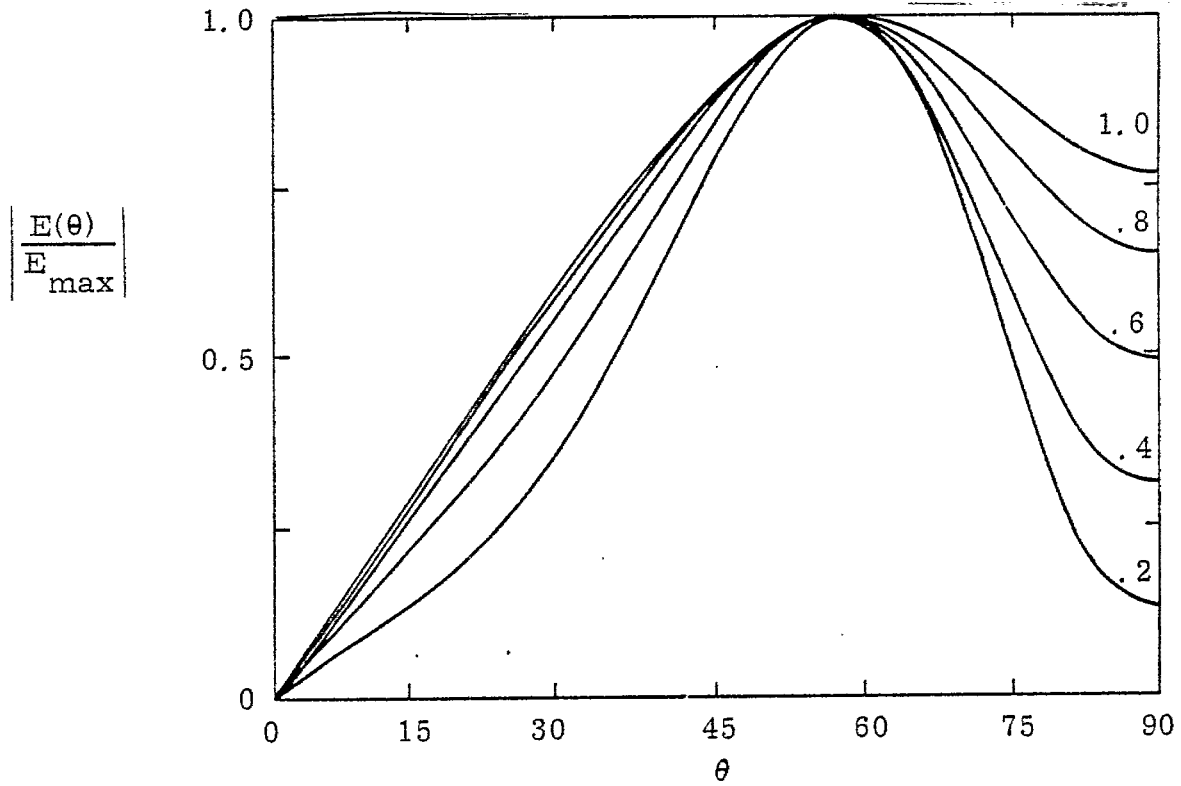


Figure 10. Normalized Radiation Pattern at $kh = 2\pi$ with $\delta = .2, .4, .6, .8, 1.0$

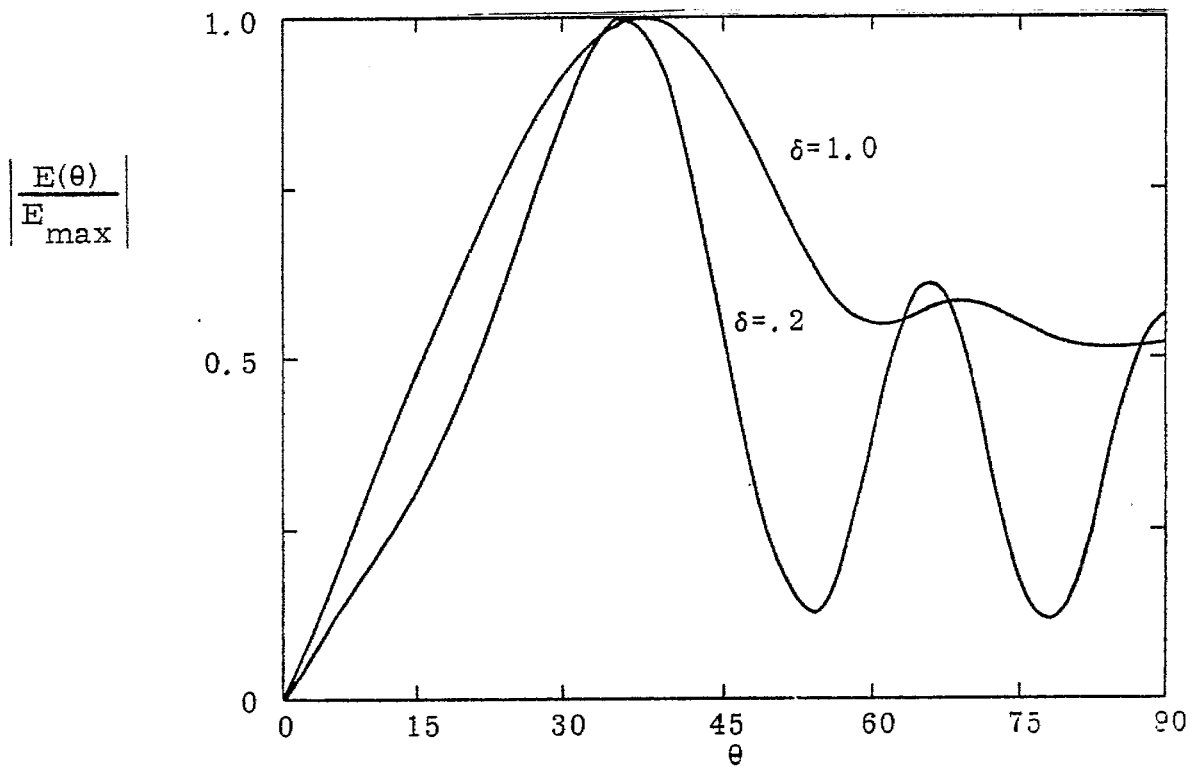


Figure 11. Normalized Radiation Pattern for $kh = 5\pi$ and $\delta = .2, 1.0$

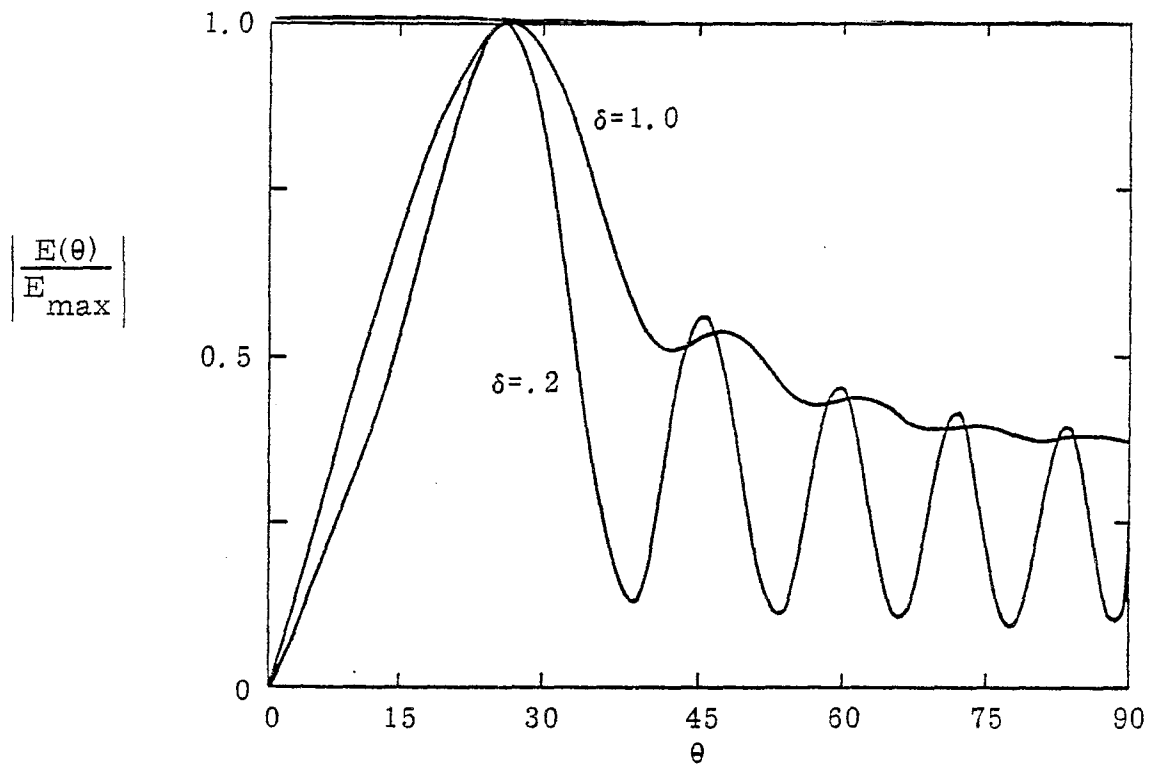


Figure 12. Normalized Radiation Pattern for $kh = 10\pi$ and $\delta = .2, 1.0$

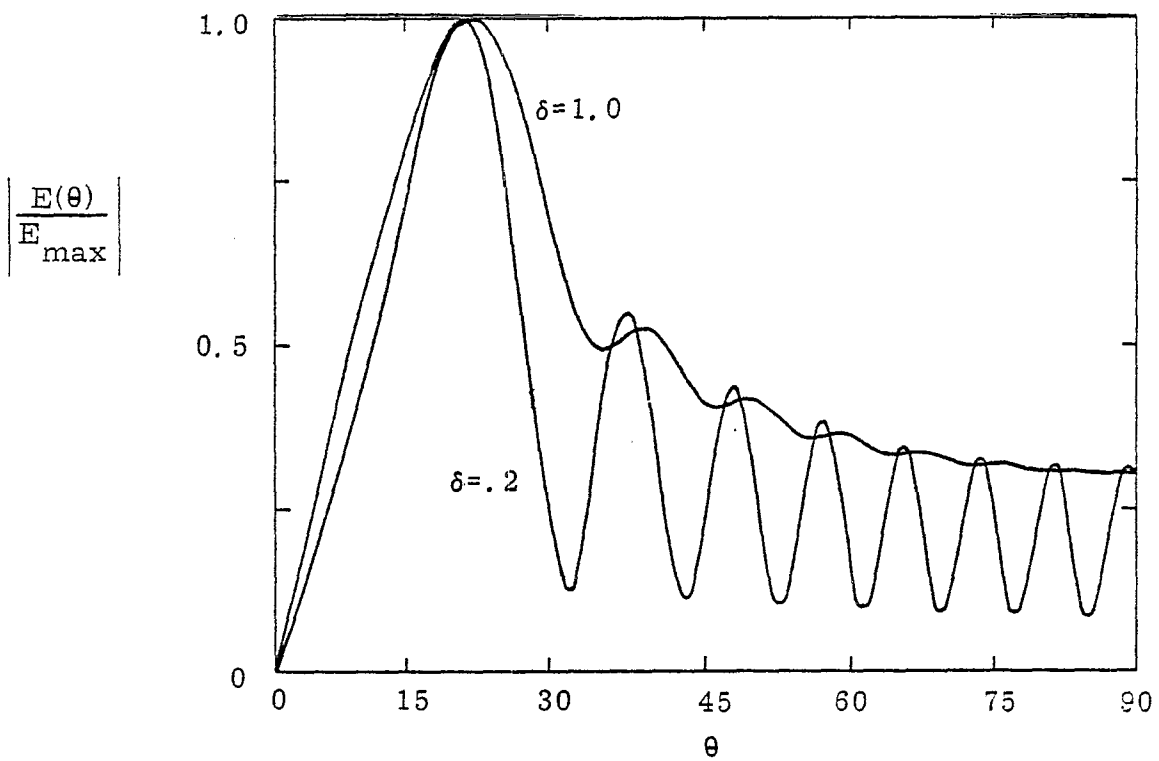


Figure 13. Normalized Radiation Pattern for $kh = 15\pi$ and $\delta = .2, 1.0$

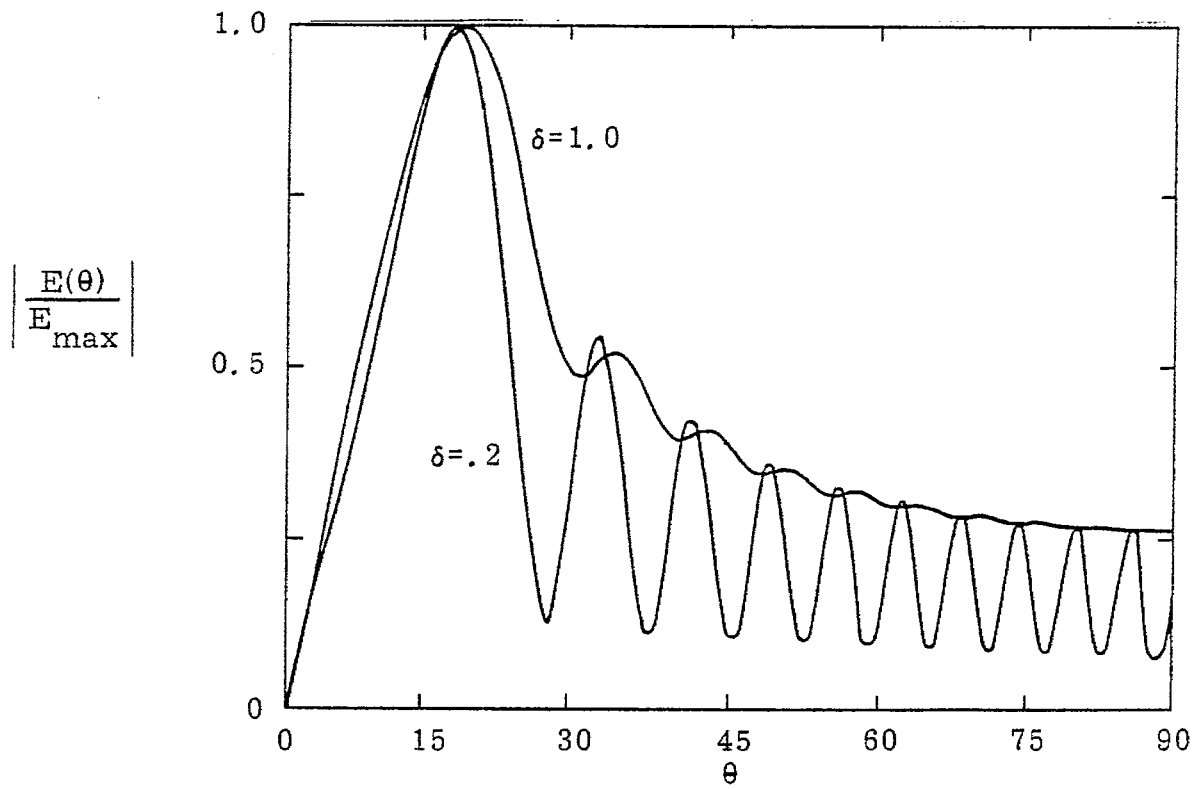


Figure 14. Normalized Radiation Pattern for $kh = 20\pi$ and $\delta = .2, 1.0$

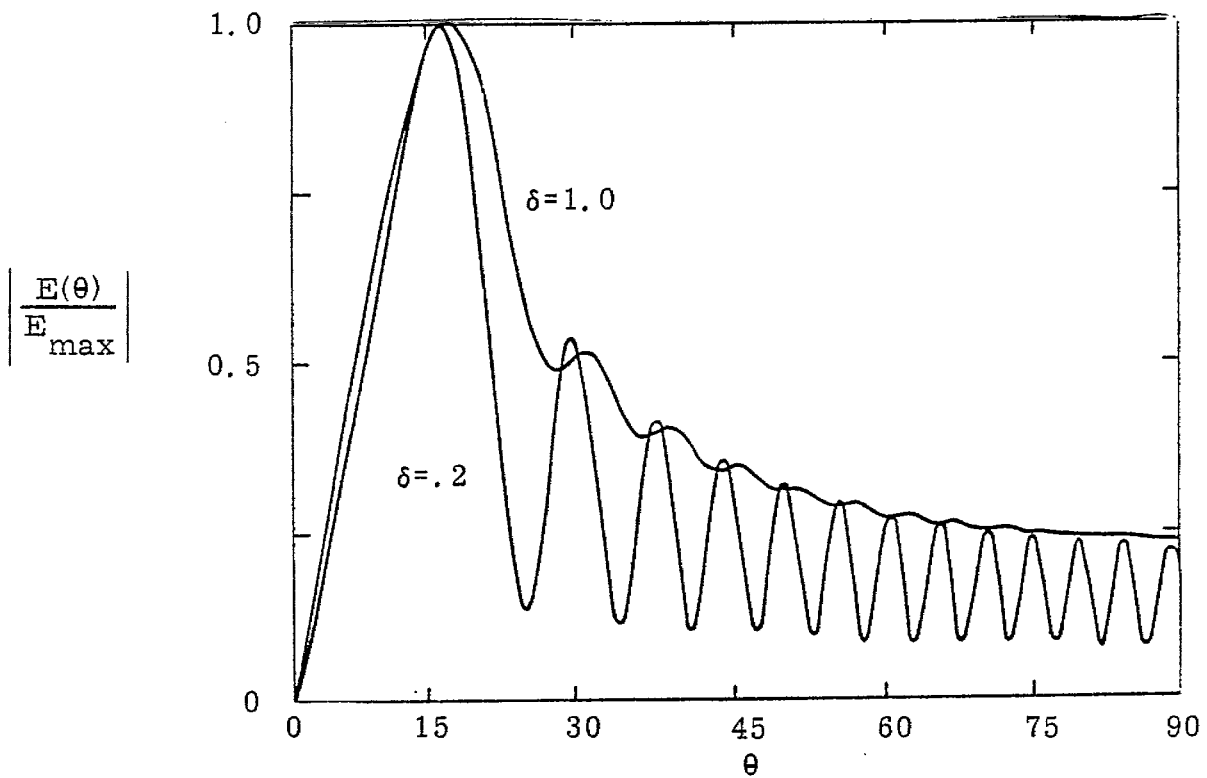


Figure 15. Normalized Radiation Pattern for $kh = 25\pi$ and $\delta = .2, 1.0$

V. Analytic Studies of Frequency Domain Radiated Field

Consider the integrand of equation 28. We replace the Kummer function by its series definition as given by equation 13.1.2 in Abramowitz and Stegun.⁶

$$\begin{aligned} M \left[-2\gamma_0 (h - |z'|) \right] &\equiv M \left[1-\delta, 2; -2\gamma_0 (h - |z'|) \right] = M(a, b; z) \\ &\equiv \sum_{n=0}^{\infty} \frac{(a)_n z^n}{(b)_n n!} \end{aligned} \quad (29)$$

with $a = 1 - \delta$, $b = 2$, $z = -2\gamma_0 (h - |z'|)$, and with

$$(a)_n \equiv a(a+1)(a+2) \cdots (a+n-1), \quad (a)_0 \equiv 1 \quad (30)$$

Using equation 29, the integral part of equation 28 may be written as

$$\mathcal{L}_\delta(s, \theta) = \int_{-h}^h \left[1 - \frac{|z'|}{h} \right] \sum_{n=0}^{\infty} \frac{(1-\delta)_n (-2\gamma_0 (h - |z'|))^n}{(2)_n n!} e^{\frac{s}{c}(-|z'| + z' \cos \theta)} dz' \quad (31)$$

Interchanging the order of integration and summation and changing the range of integration to $[0, h]$ gives us

$$\begin{aligned} \mathcal{L}_\delta(s, \theta) &= \sum_{n=0}^{\infty} \frac{(1-\delta)_n (-2\gamma_0)^n}{(2)_n n! h} \int_0^h (h-z')^{n+1} e^{-\frac{s}{c} z'} \left(e^{-\frac{s z'}{c} \cos \theta} + e^{\frac{s z'}{c} \cos \theta} \right) dz' \\ &= \sum_{n=0}^{\infty} \chi_n(s) \mathcal{L}'_n(s, \theta) \end{aligned} \quad (32)$$

where \mathcal{L}' represents only the integral part of equation 32 and χ represents the factor in front of the integral. If we change variables in $\mathcal{L}'_n(s, \theta)$ by letting

$$\begin{aligned} \nu &= h - z' \\ p &= \frac{S}{c} (1 + \cos \theta) \\ q &= \frac{S}{c} (1 - \cos \theta) \end{aligned} \tag{33}$$

Then $\mathcal{L}'_n(s, \theta)$ becomes

$$\mathcal{L}'_n(s, \theta) = \int_0^h \nu^{n+1} \left(e^{p(\nu-h)} + e^{q(\nu-h)} \right) d\nu \tag{34}$$

\mathcal{L}'_n may then be expressed as the sum of two integrals each of the form

$$\int_0^a x^n e^{bx} dx = \frac{(-1)^{n+1} n!}{b^{n+1}} + \frac{e^{ab}}{b} \sum_{j=0}^n (-1)^j \frac{n! a^{n-j}}{(n-j)! b^j} \tag{35}$$

Thus if we watch our p's and q's, equation 32 becomes

$$\mathcal{L}_\delta(s, \theta) = \sum_{n=0}^{\infty} \left[\frac{(1-\delta)_n (-2\gamma_0)^n}{(2)_n n! h} \right]$$

$$x \left\{ e^{-ph} \left(\frac{(-1)^{n+2} (n+1)!}{p^{n+2}} + \frac{e^{ph}}{p} \sum_{j=0}^{n+1} (-1)^j \frac{(n+1)! h^{n+1-j}}{(n+1-j)! p^j} \right) \right. \quad (36)$$

$$\left. + e^{-qh} \left(\frac{(-1)^{n+2} (n+1)!}{q^{n+2}} + \frac{e^{qh}}{q} \sum_{j=0}^{n+1} (-1)^j \frac{(n+1)! h^{n+1-j}}{(n+1-j)! q^j} \right) \right]$$

Equation 28 may then be written as

$$\tilde{\xi}(\theta) = \frac{\sin\theta}{2} \frac{s}{[\text{sh}(1-f_\delta) + c\alpha]} \frac{1}{M(-2\gamma_0 h)} \mathcal{L}_\delta(s, \theta) \quad (37)$$

with $\mathcal{L}_\delta(s, \theta)$ given by equation 36. Substituting for f_δ from equation 18 and using the relation

$$M'(a, b; z) = \frac{a}{b} M(a+1, b+1; z) \quad (38)$$

we have

$$\tilde{\xi}'(\theta) = \frac{\sin\theta}{2} \frac{s \mathcal{L}_\delta(s, \theta)}{(c\alpha + \text{sh}) M(1-\delta, 2; -2\gamma_0 h) - \text{sh}(1-\delta) M(2-\delta, 3; -2\gamma_0 h)} \quad (39)$$

and substituting for the M 's gives us

$$\tilde{\xi}'(\theta) = \frac{\sin\theta}{2} \frac{s \mathcal{L}_0(s, \theta)}{\left\{ (\alpha + sh) \sum_{n=0}^{\infty} \frac{(1-\delta)_n (-2\gamma_0 h)^n}{(2)_n n!} - sh(1-\delta) \sum_{n=0}^{\infty} \frac{(2-\delta)_n (-2\gamma_0 h)^n}{(3)_n n!} \right\}}$$

(40)

Recalling that $\gamma_0 = s/c$, $p = s/c(1+\cos\theta)$, $q = s/c(1-\cos\theta)$, we see that aside from factors of the form $\exp[-s_h(1 \pm \cos\theta)]$ both numerator and denominator are made up of infinite series in powers of s . This remains true for arbitrary continuous passive element loading (with the $[h-|z'|]^{-1}$ functional form of course). The exponentials correspond to time retardation in the time domain.

VI. Analysis of Special Cases

Although for a general δ corresponding to some loading on the antenna, equation 40 with $\mathcal{L}_\delta(s, \theta)$ defined by equation 36 appears quite forbidding, there are special cases of interest for which further simplifications and analyses have been accomplished. If we choose δ to be a positive integer, corresponding to certain cases of purely resistive loading, the various infinite series will all become finite polynomials which may, in principle at least, be analytically transformed into the time domain. If δ is a positive integer, equations 36 and 40 are unchanged except that ∞ as an upper limit on the range of summations is replaced by $\delta-1$ on those summations. Three special cases are given below with $\delta = 0, 1, 2$.

$$1. \quad \delta = 0, \quad \theta = \frac{\pi}{2}$$

For the $\delta = 0$ case, we go back to the integral definition for $\mathcal{L}_0(s, \theta)$, namely

$$\mathcal{L}_0(s, \theta) = \frac{1}{h} \int_{-h}^h (h - |z'|) M \left[1, 2; -2\gamma_0(h - |z'|) \right] e^{\gamma_0(-|z'| + z' \cos \theta)} dz' \quad (41)$$

Using the relation

$$M(1, 2; 2z) = \frac{e^z}{z} \sin z \quad (42)$$

which is equation 13.6.14 in Abramowitz and Stegun⁶, specializing to the $\theta = \frac{\pi}{2}$ case and with $\eta = -\gamma_0(h - z')$ we obtain

$$\begin{aligned}
\mathcal{L}_0(s, \theta) &= - \frac{1}{\gamma_0} \int_{-\gamma_0 h}^0 (e^{2\eta} - 1) e^{-\gamma_0 h} e^{-\eta} d\eta \\
&= \frac{1}{h\gamma_0} \left[1 - e^{-\gamma_0 h} \right]^2
\end{aligned} \tag{43}$$

In the denominator of equation 39 we may use a recursion relation, namely

$$\begin{aligned}
M(a+1, b+1; z) &= \frac{1}{az} \left\{ b(1-b+z) M(a, b; z) \right. \\
&\quad \left. + b(b-1) M(a-1, b-1; z) \right\}
\end{aligned} \tag{44}$$

which is equation 13.4.7 in Abramowitz and Stegun⁶ to obtain

$$M(2, 3; -2\gamma_0 h) = \frac{1}{\gamma_0 h} \left\{ (1+2\gamma_0 h) M(1, 2; -2\gamma_0 h) - 1 \right\} \tag{45}$$

so that setting $\alpha = 1 + \frac{C_g}{C_a} \approx 1$ for $C_g \gg C_a$,

$$(c+sh) M(1, 2; -2\gamma_0 h) - sh M(2, 3; -2\gamma_0 h) = \frac{c}{2} \left[e^{-2\gamma_0 h} + 1 \right] \tag{46}$$

Thus, for $\delta = 0$, $\theta = \frac{\pi}{2}$, and $\alpha = 1$, we obtain

$$\xi_1\left(\frac{\pi}{2}\right) = \frac{1}{\gamma_0 h} \frac{\left[\frac{1 - e^{-\gamma_0 h}}{e^{-2\gamma_0 h} + 1} \right]^2}{(47)}$$

which agrees with equation 44 of reference 3 with $\beta = 0$, $\alpha = 1$. Following Baum we may expand this result as a geometric series giving

$$\begin{aligned} \xi_1\left(\frac{\pi}{2}\right) &= \frac{1}{\gamma_0 h} \left[1 - 2e^{-\gamma_0 h} + e^{-2\gamma_0 h} \right] \sum_{n=0}^{\infty} (-1)^n e^{-2n\gamma_0 h} \\ &= \frac{1}{s_h} \left\{ 1 + 2 \sum_{n=0}^{\infty} (-1)^n e^{-(2n+1)\gamma_0 h} \right\} \end{aligned} \quad (48)$$

So that

$$\xi_1\left(\frac{\pi}{2}\right) = u(\tau_h) + 2 \sum_{n=1}^{\infty} (-1)^n u\left[\tau_h - (2n-1)\right] \quad (49)$$

where $u(t)$ is the unit step function.

The result in equation 49 is simply an undamped square wave for $\tau_h > 0$ and is not a precise result for the radiating cylindrical antenna since the model ignores radiation damping, but it is the result of the transmission line model in the no loading limit. One would expect that the deviation between the result obtained in the transmission line model and that of a more accurate model would be greatest for the no loading case. For resistively loaded cases, except perhaps for very early times, the transmission line approximation results should become more accurate as the loading increases.

2. $\delta = 1$

For this case, using equations 40 and 36 with only the $n=0$ term in each summation, we obtain

$$\begin{aligned} \tilde{\xi}'(\theta) = \frac{\sin\theta}{2(s_h + \alpha)} & \left\{ \frac{1}{(1+\cos\theta)} \left[\frac{e^{-s_h(1+\cos\theta)}}{s_h(1+\cos\theta)} + 1 \right] \right. \\ & \left. + \frac{1}{(1-\cos\theta)} \left[\frac{e^{-s_h(1-\cos\theta)}}{s_h(1-\cos\theta)} + 1 \right] \right\} = \frac{2\pi f_g r \tilde{E}_{f\theta}}{t_h V_o} e^{\gamma_o r} \end{aligned} \quad (50)$$

This result is identical to equation 77 of reference 3. Therefore, the inverse transform time domain result is

$$\begin{aligned} \xi'(\theta) = \frac{\sin(\theta)}{2} & \left\{ \left[\frac{e^{-\alpha\tau_h}}{1-\cos(\theta)} - \frac{1-e^{-\alpha\tau_h}}{\alpha(1-\cos(\theta))^2} \right] u(\tau_h) \right. \\ & + \frac{1}{\alpha} \frac{1-e^{-\alpha[\tau_h-(1-\cos(\theta))]}}{(1-\cos(\theta))^2} u(\tau_h - [1-\cos(\theta)]) \\ & + \left[\frac{e^{-\alpha\tau_h}}{1+\cos(\theta)} - \frac{1-e^{-\alpha\tau_h}}{\alpha(1+\cos(\theta))^2} \right] u(\tau_h) \\ & \left. + \frac{1}{\alpha} \frac{1-e^{-\alpha[\tau_h-(1+\cos(\theta))]}}{(1+\cos(\theta))^2} u(\tau_h - [1+\cos(\theta)]) \right\} \\ & = 2\pi f_g \frac{r E_{f\theta}}{V_o} \end{aligned} \quad (51)$$

3. $\delta = 2$

For this case the frequency domain result is

$$\begin{aligned} \tilde{\omega}'(\theta) &= \frac{\sin\theta}{2} \frac{s_h}{[(s_h(s_h+2)+\alpha(s_h+1))]} \\ &\times \left\{ \left(1 - \frac{2}{1-\cos\theta}\right) \left[\frac{e^{-s_h(1-\cos\theta)}}{s_h^2(1-\cos\theta)^2} - \frac{1}{s_h(1-\cos\theta)} \right] + \frac{1}{(1-\cos\theta)} \right. \\ &\left. + \left(1 - \frac{2}{1+\cos\theta}\right) \left[\frac{e^{-s_h(1+\cos\theta)}}{s_h^2(1+\cos\theta)^2} - \frac{1}{s_h(1+\cos\theta)} \right] + \frac{1}{(1+\cos\theta)} \right\} \end{aligned} \quad (52)$$

If we write

$$s_h(s_h+2) + \alpha(s_h+1) = s_h^2 + (\alpha+2)s_h + \alpha = (s_h + \alpha')(s_h + \frac{\alpha}{\alpha'}) \quad (53)$$

where $\alpha' = \frac{\alpha}{2} + 1 + \sqrt{\left(\frac{\alpha}{2}\right)^2 + 1}$

we may rewrite equation 52 in the form

$$\begin{aligned} \tilde{\omega}'(\theta) &= \frac{\sin\theta}{2} \frac{1}{(s_h + \alpha')(s_h + \frac{\alpha}{\alpha'})} \\ &\times \left\{ - \frac{(1+\cos\theta)}{(1-\cos\theta)^3} \frac{e^{-s_h(1-\cos\theta)}}{s_h} + \frac{s_h^2(1-\cos\theta)^2 - s_h \sin^2\theta + (1+\cos\theta)}{s_h(1-\cos\theta)^3} \right. \\ &\left. - \frac{(1-\cos\theta)}{(1+\cos\theta)^3} \frac{e^{-s_h(1+\cos\theta)}}{s_h} + \frac{s_h^2(1+\cos\theta)^2 - s_h \sin^2\theta + (1-\cos\theta)}{s_h(1+\cos\theta)^3} \right\} \end{aligned} \quad (54)$$

Taking the inverse transform, the time domain waveform becomes

$$\begin{aligned}
 \xi'(\theta) = & \frac{\sin\theta}{2} \left\{ - \frac{1+\cos\theta}{(1-\cos\theta)^3} \left[\frac{\alpha' \left(1 - e^{-\frac{\alpha}{\alpha'} [\tau_h - (1-\cos\theta)]} \right) - \frac{\alpha}{\alpha'} \left(1 - e^{-\alpha' [\tau_h - (1-\cos\theta)]} \right)}{\alpha \left(\alpha' - \frac{\alpha}{\alpha'} \right)} \right] \right. \\
 & \cdot u [\tau_h - (1-\cos\theta)] + \left[\frac{1+\cos\theta}{\alpha(1-\cos\theta)^3} + \frac{\alpha'^2(1-\cos\theta)^2 + \alpha' \sin^2 \theta + (1+\cos\theta)}{\alpha' \left(\alpha' - \frac{\alpha}{\alpha'} \right) (1-\cos\theta)^3} e^{-\alpha' \tau_h} \right. \\
 & + \frac{\left(\frac{\alpha}{\alpha'} \right)^2 (1-\cos\theta)^2 + \frac{\alpha}{\alpha'} \sin^2 \theta + (1+\cos\theta)}{\left(\frac{\alpha}{\alpha'} \right) \left(\frac{\alpha}{\alpha'} - \alpha' \right) (1-\cos\theta)^3} e^{-\frac{\alpha}{\alpha'} \tau_h} \\
 & + \frac{1-\cos\theta}{\alpha(1+\cos\theta)^3} + \frac{\alpha'^2(1+\cos\theta)^2 + \alpha' \sin^2 \theta + (1-\cos\theta)}{\alpha' \left(\alpha' - \frac{\alpha}{\alpha'} \right) (1+\cos\theta)^3} e^{-\alpha' \tau_h} \\
 & \left. + \frac{\left(\frac{\alpha}{\alpha'} \right)^2 (1+\cos\theta)^2 + \frac{\alpha}{\alpha'} \sin^2 \theta + (1-\cos\theta)}{\left(\frac{\alpha}{\alpha'} \right) \left(\frac{\alpha}{\alpha'} - \alpha' \right) (1+\cos\theta)^3} e^{-\frac{\alpha}{\alpha'} \tau_h} \right] u(\tau_h) \\
 & - \frac{1-\cos\theta}{(1+\cos\theta)^3} \left[\frac{\alpha' \left(1 - e^{-\frac{\alpha}{\alpha'} [\tau_h - (1+\cos\theta)]} \right) - \frac{\alpha}{\alpha'} \left(1 - e^{-\alpha' [\tau_h - (1+\cos\theta)]} \right)}{\alpha \left(\alpha' - \frac{\alpha}{\alpha'} \right)} \right] \\
 & \left. \cdot u [\tau_h - (1+\cos\theta)] \right\} \tag{55}
 \end{aligned}$$

Note the symmetries with respect to the roots α' and α/α' of the quadratic $[s_h(s_h+2)+\alpha(s_h+1)]$. If we further specialize to $\theta = \frac{\pi}{2}$, $\alpha = 1$, we obtain

$$\xi' \left(\frac{\pi}{2} \right) = \left\{ - \left[\alpha'^2 \left(1 - e^{-(\tau_h-1)/\alpha'} \right) - \left(1 - e^{-\alpha'(\tau_h-1)} \right) \right] u(\tau_h-1) + \left[\alpha'^2 - 1 + (\alpha'^2 + \alpha' + 1) \left(e^{-\alpha'\tau_h} - e^{-\tau_h/\alpha'} \right) \right] u(\tau_h) \right\} \frac{1}{\alpha'^2 - 1} \quad (56)$$

This waveform has a zero at $\tau_h \cong .51$ and a minimum of $\xi' \cong -0.1$ at $\tau_h \cong .86$. The value of α' for $\alpha=1$ is $\alpha' = \frac{3+\sqrt{5}}{2} \cong 2.618$. Although no curves were obtained directly from equations 54, 55 or 56, the numerical results of the general routine as presented in figures 18 through 21 agree very well with the analytical results.

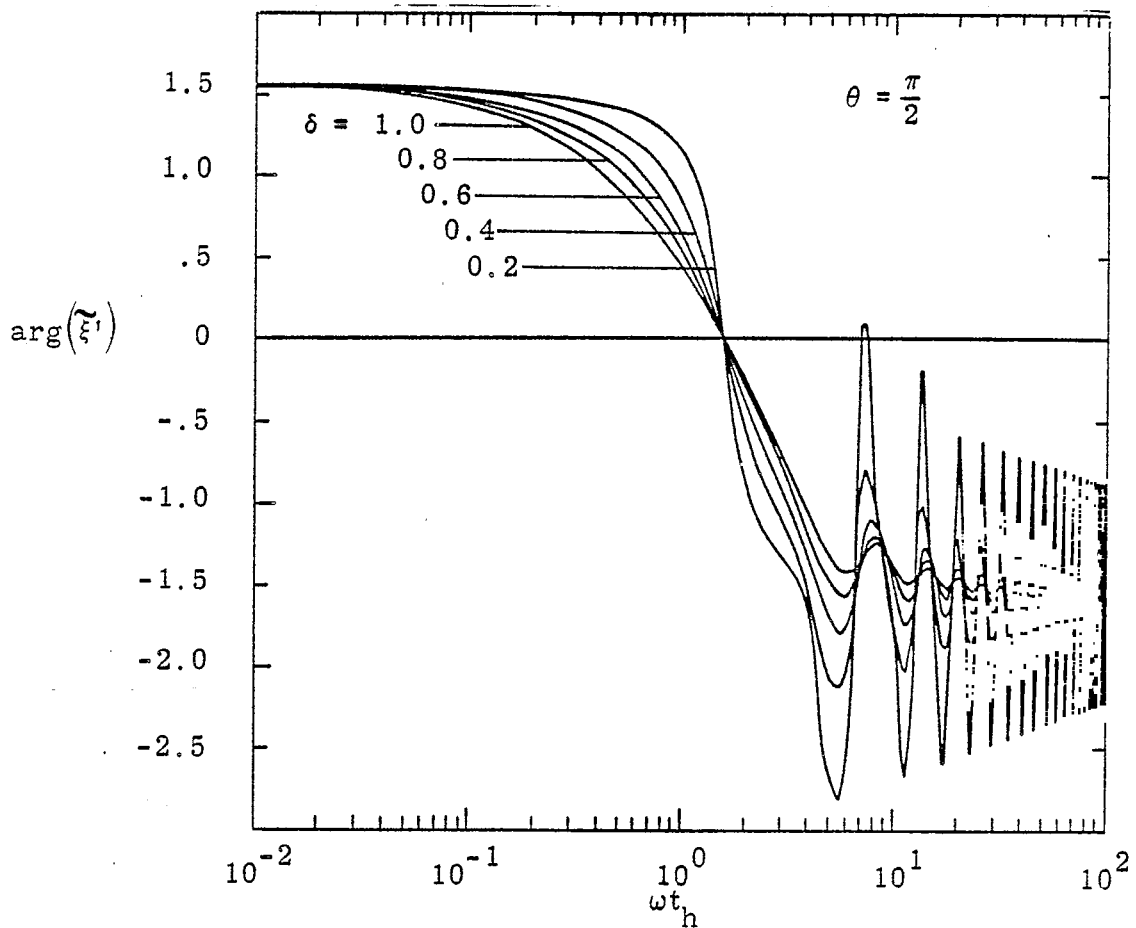
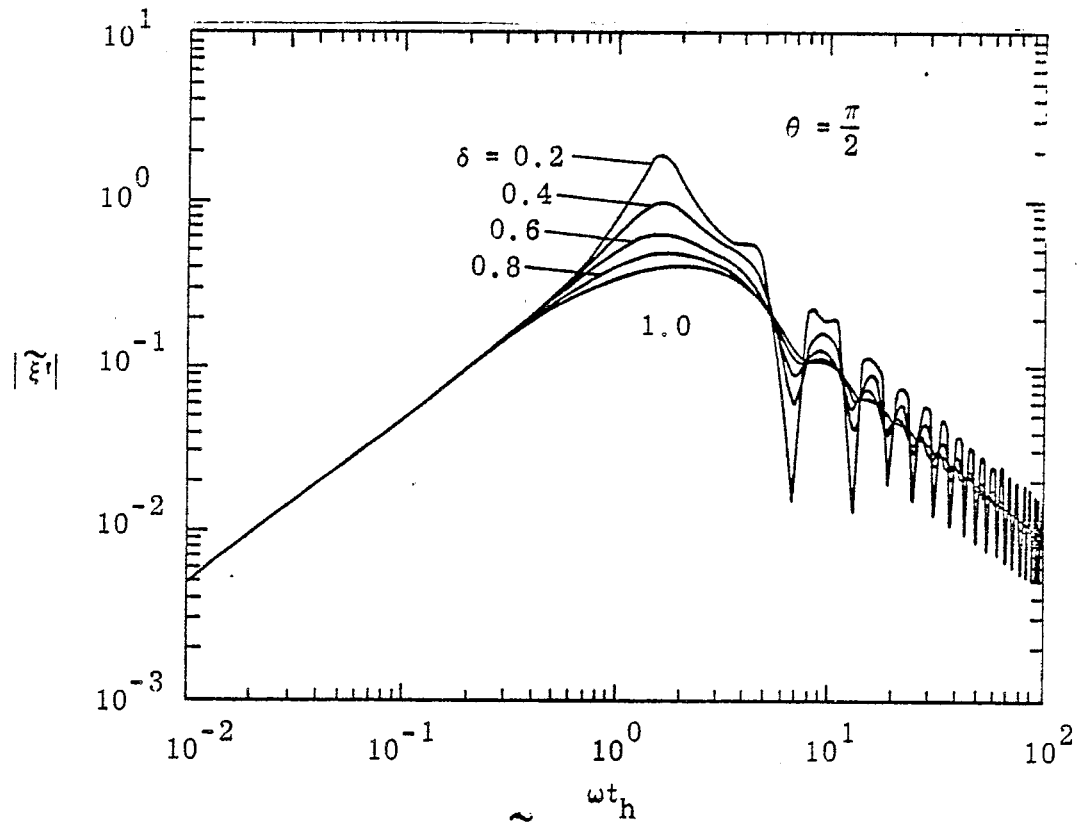
In theory, it is possible to continue to higher integer values of δ , but finding roots algebraically becomes increasingly clumsy, and attempting analytical inversions to get the time domain result becomes correspondingly less attractive. Since these special cases do agree well with the results calculated by the general routine, they lend confidence to the other results obtained for which an analytic closed form solution is not available or convenient.

VII. Numerical Results

Figures 16 and 17 give $\tilde{\xi}'$ and ξ' for the loading parameter δ ranging between .2 and 1.0 for a fixed observer angle of $\frac{\pi}{2}$. We see that as δ is diminished from 1 toward 0, the first zero crossing moves toward 1 and the undershoot also increases. Physically, what is happening is that for lightly loaded cases we are approaching the lossless transmission line solution which is +1 from $0 < \tau_h < 1$, jumps discontinuously from +1 to -1 at $\tau_h = 1$, stays at -1 until $\tau_h = 3$, and jumps back to +1 at that point. The lossless case is given by equation 49. Figures 18 through 31 give normalized frequency and time domain radiated E field for various resistive loading corresponding to values of δ between 0.2 and 3 with the observer angle θ as a parameter. It may be observed that for very early times the radiated field goes as $(\sin \theta)^{-1}$; however, for late times the dependence is $\sin \theta$. The dependence on θ is discussed in reference 3. We may note that the effects of the antenna ends on the radiated field are progressively smoothed as one increases the loading at the cost of damping the radiated field more rapidly and decreasing the time of first zero crossing. Also the time of arrival of the end effects is a function of observer angle. Remembering that we are in the far zone of the antenna, $\frac{r}{2h} \gg 1$ where r is distance from the antenna center to the observation point and $2h$ is the antenna length. It may be calculated that at $\theta = \frac{\pi}{2}$, end effects are simultaneous at $\tau_h = 1$, at $\theta = \frac{\pi}{3}$ end effects appear at $\tau_h = .5$ and 1.5; and at $\theta = \frac{\pi}{6}$ end effects occur at $\tau_h = .134$ and 1.866. For example, see figures 19, 21, 23, 25, and 27. For $\delta = 2, 3$ the discontinuities in the slope of ξ' have been removed at the cost of damping the waveform more rapidly.

Other cases of interest arise when δ is a complex number. If we consider the equivalent transmission line to have an inductive load per unit length

$$L' = \frac{2Z_{\infty}}{h - |z'|} \tau_h \lambda = 2\mu_0 f_g \left[1 - \frac{|z'|}{h} \right]^{-1} \lambda \quad (57)$$



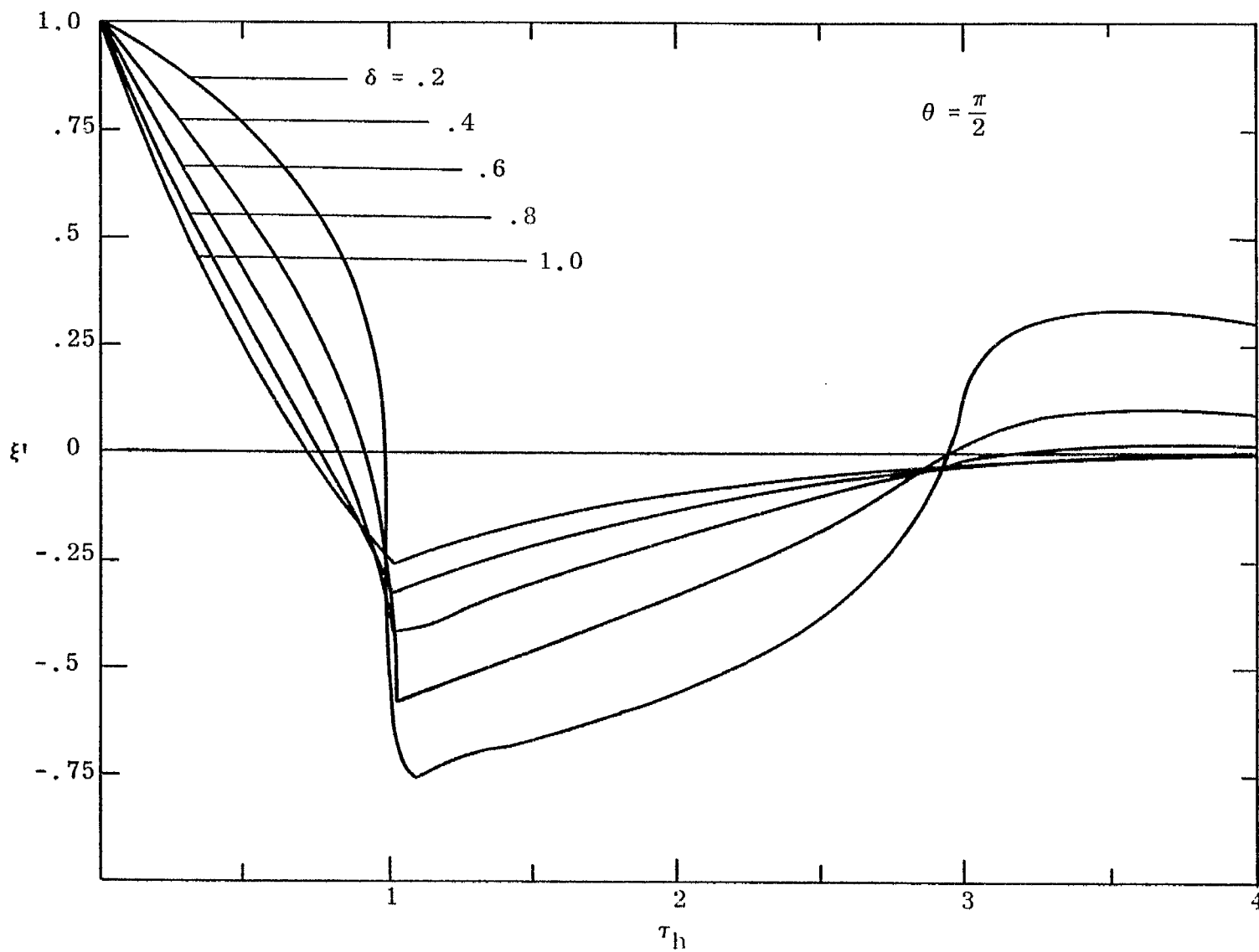


Figure 17. ξ' for $\delta = .2, .4, .6, .8, 1.0$

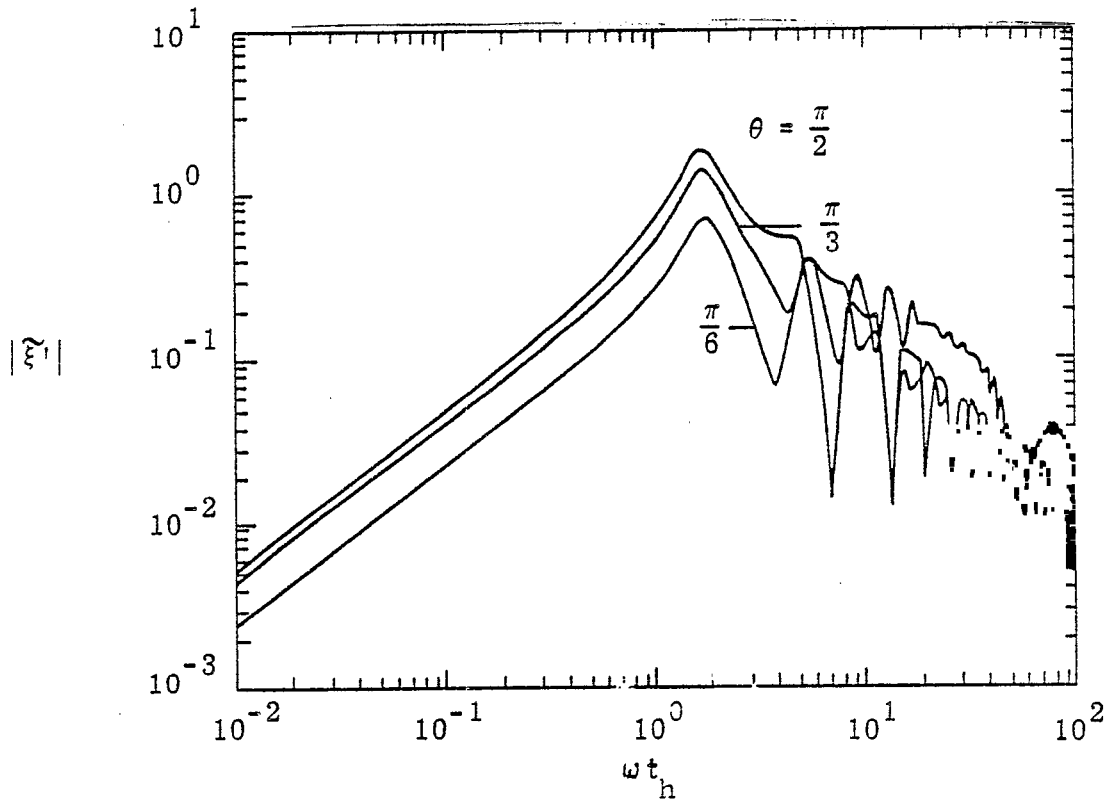


Figure 18a. $|\tilde{\xi}'|$ for $\theta = \frac{\pi}{2}, \frac{\pi}{3}, \frac{\pi}{6}$ with $\delta = 0.2$

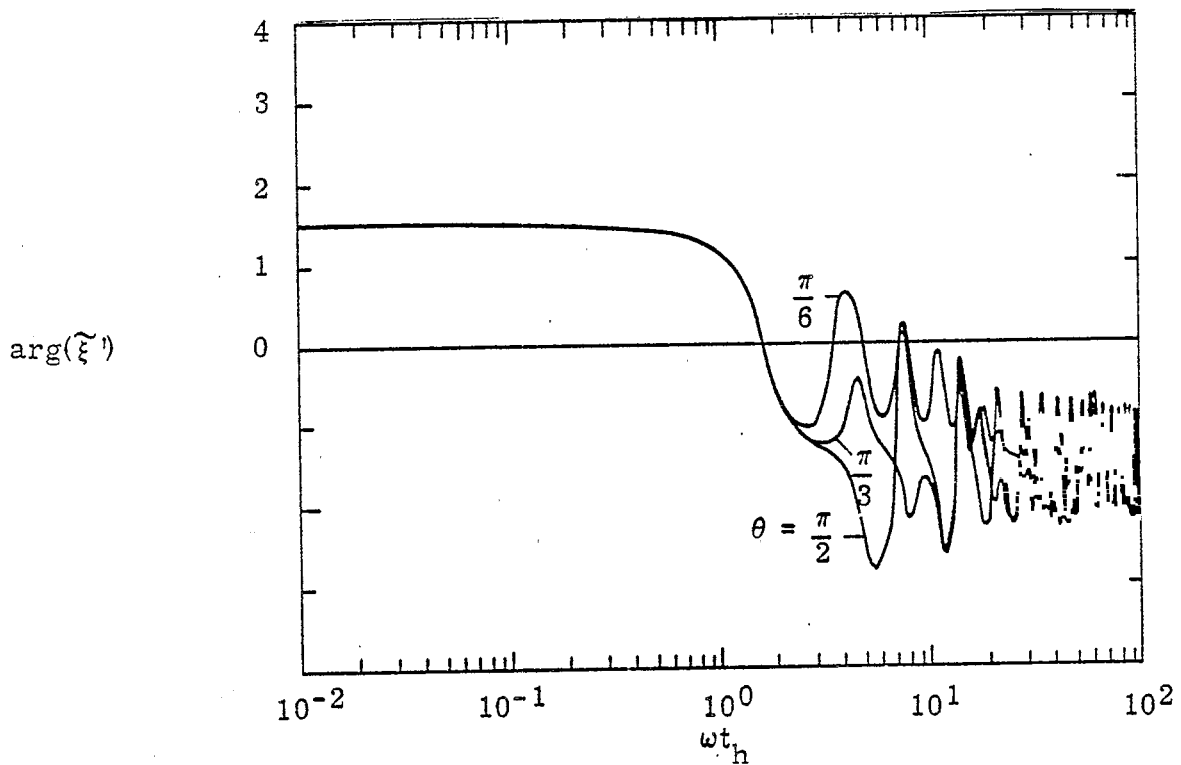


Figure 18b. Phase of $\tilde{\xi}'$ for $\theta = \frac{\pi}{2}, \frac{\pi}{3}, \frac{\pi}{6}$ with $\delta = 0.2$

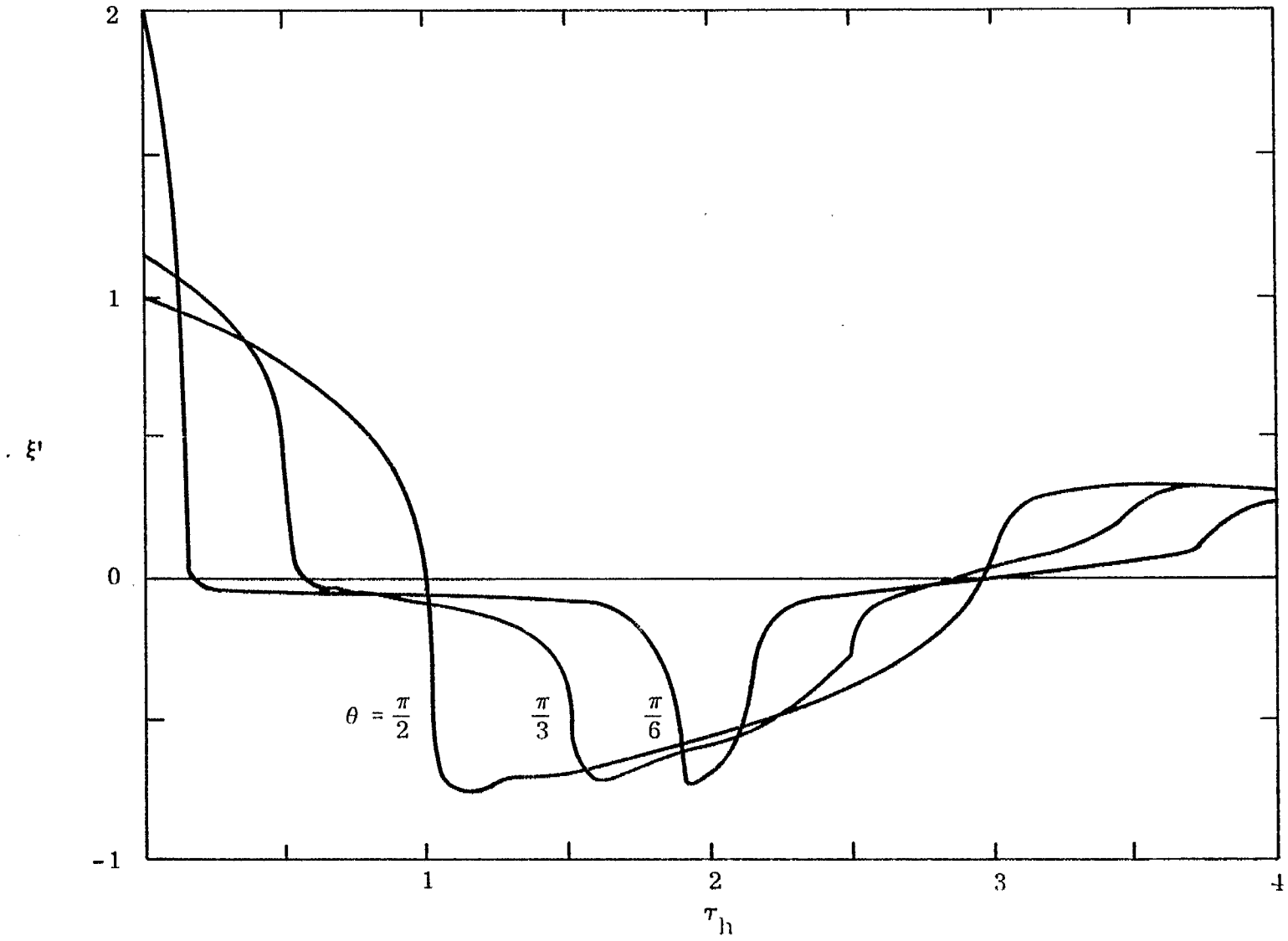


Figure 19. ξ' for $\theta = \frac{\pi}{2}, \frac{\pi}{3}, \frac{\pi}{6}$ with $\delta = 0.2$

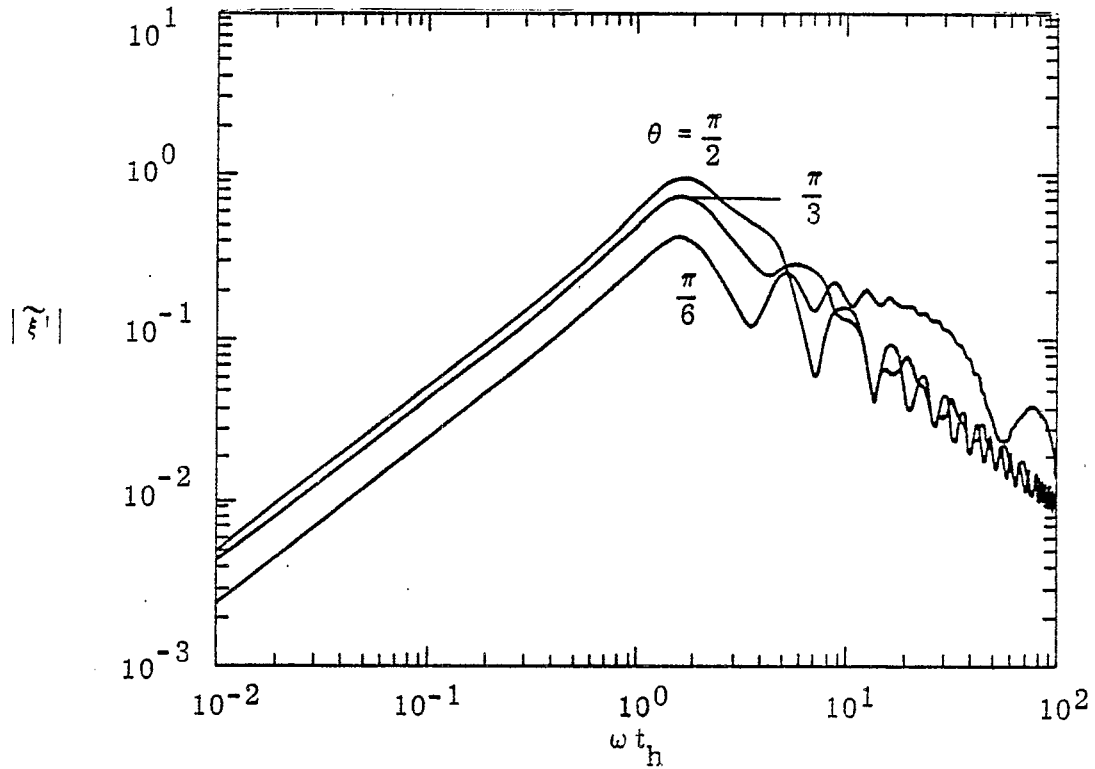


Figure 20a. $|\tilde{\xi}'|$ for $\theta = \frac{\pi}{2}, \frac{\pi}{3}, \frac{\pi}{6}$ with $\delta = 0.4$

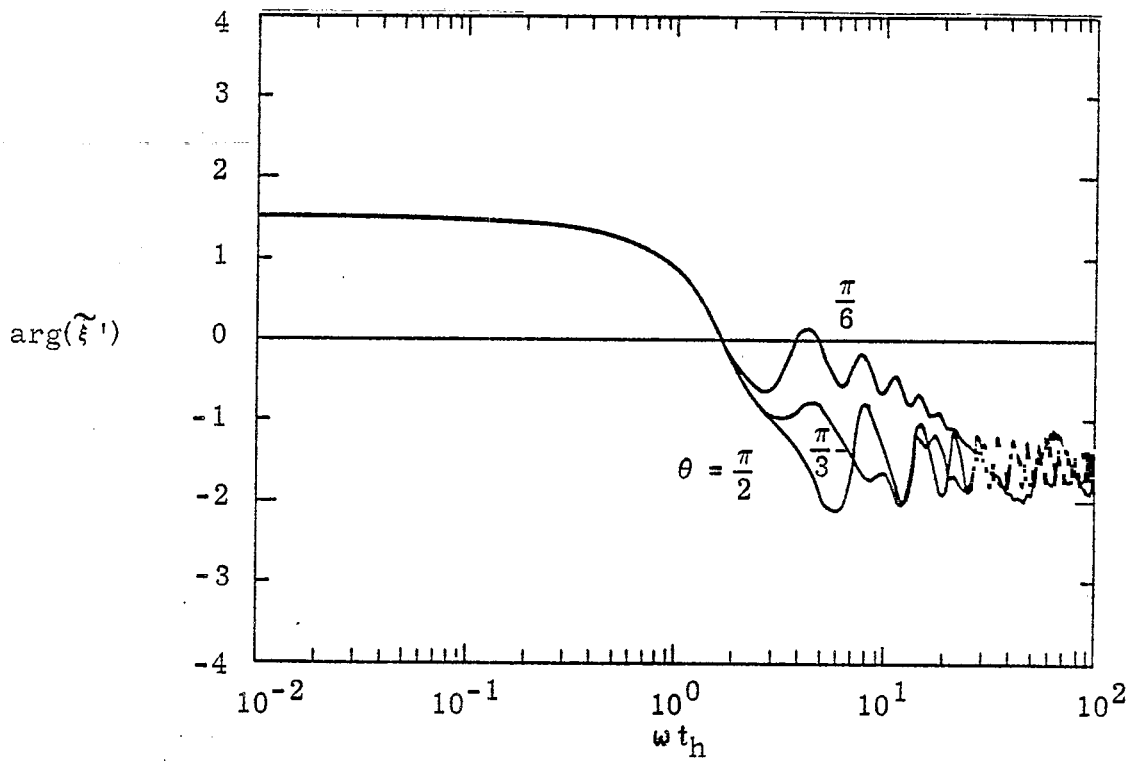


Figure 20b. Phase of $\tilde{\xi}'$ for $\theta = \frac{\pi}{2}, \frac{\pi}{3}, \frac{\pi}{6}$ with $\delta = 0.4$

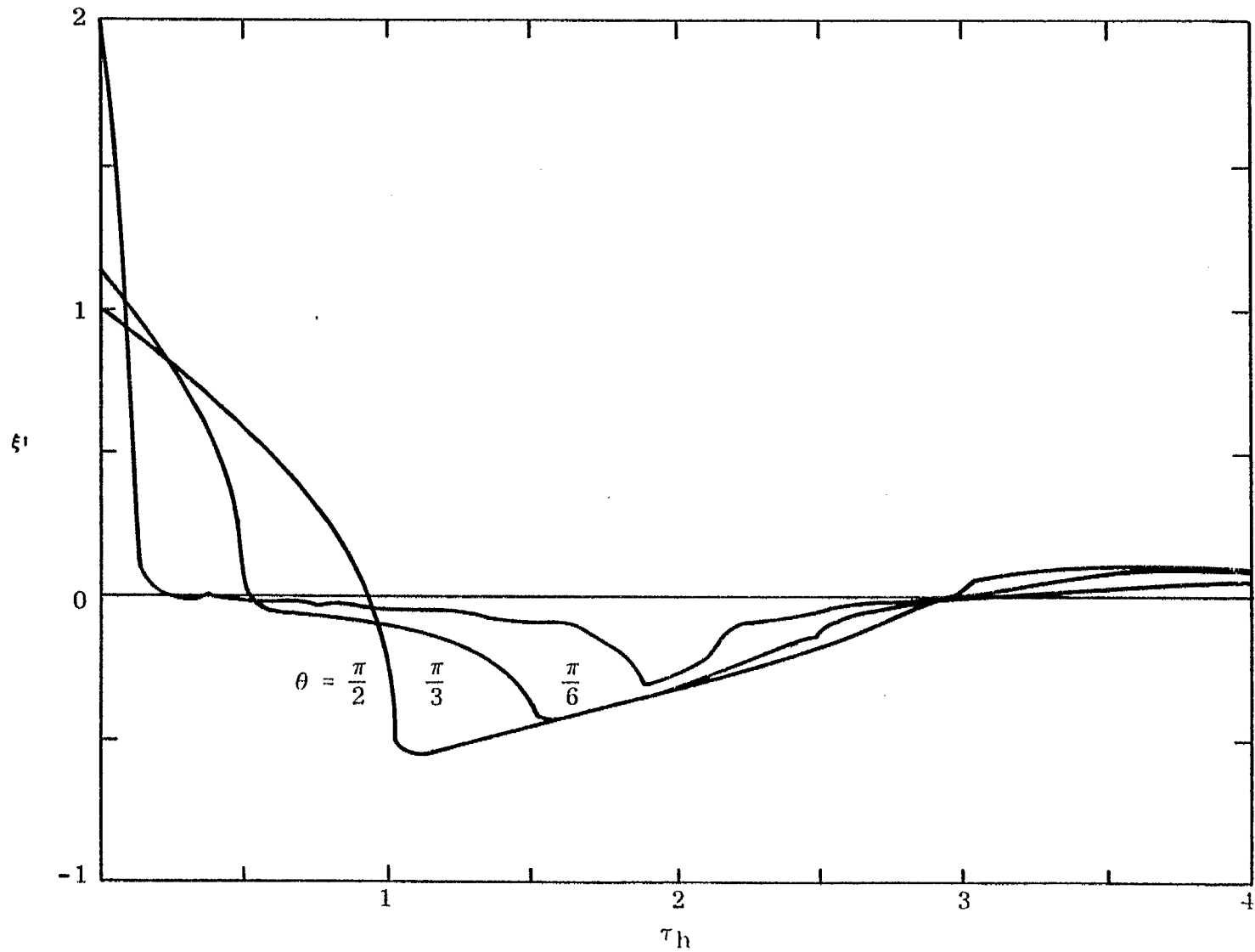


Figure 21. ξ' for $\theta = \frac{\pi}{2}, \frac{\pi}{3}, \frac{\pi}{6}$ with $\delta = 0.4$

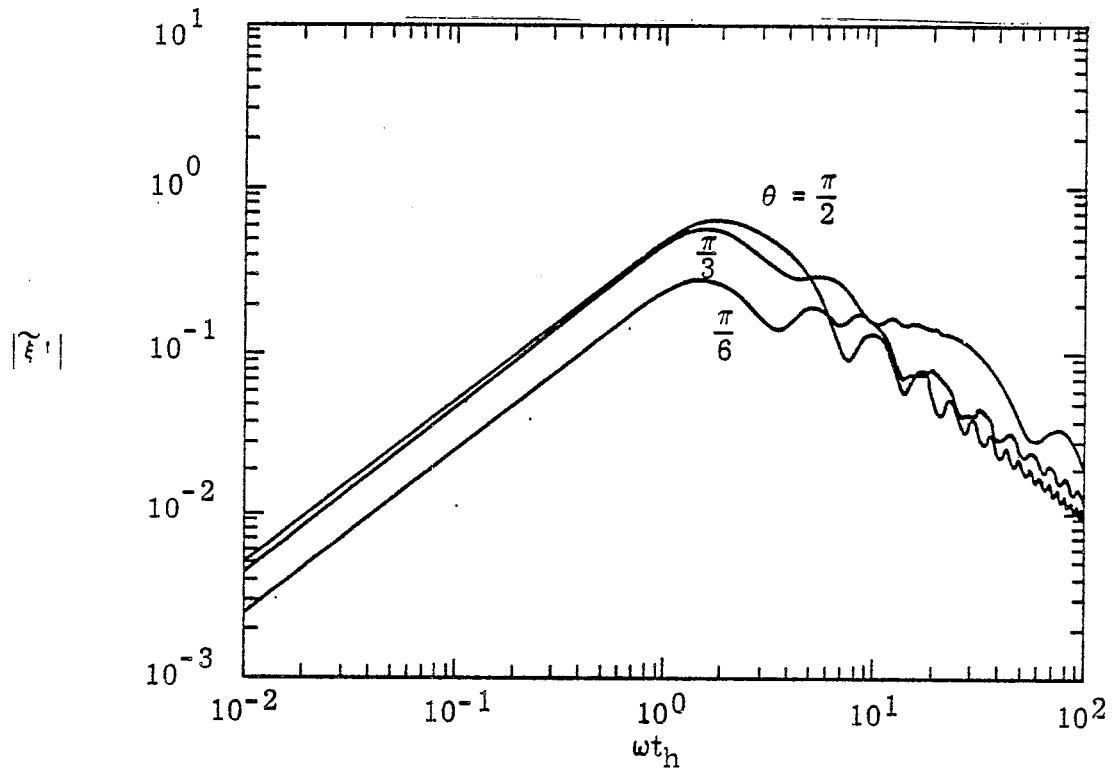


Figure 22a. $|\tilde{\xi}'|$ for $\theta = \frac{\pi}{2}, \frac{\pi}{3}, \frac{\pi}{6}$ with $\delta = 0.6$

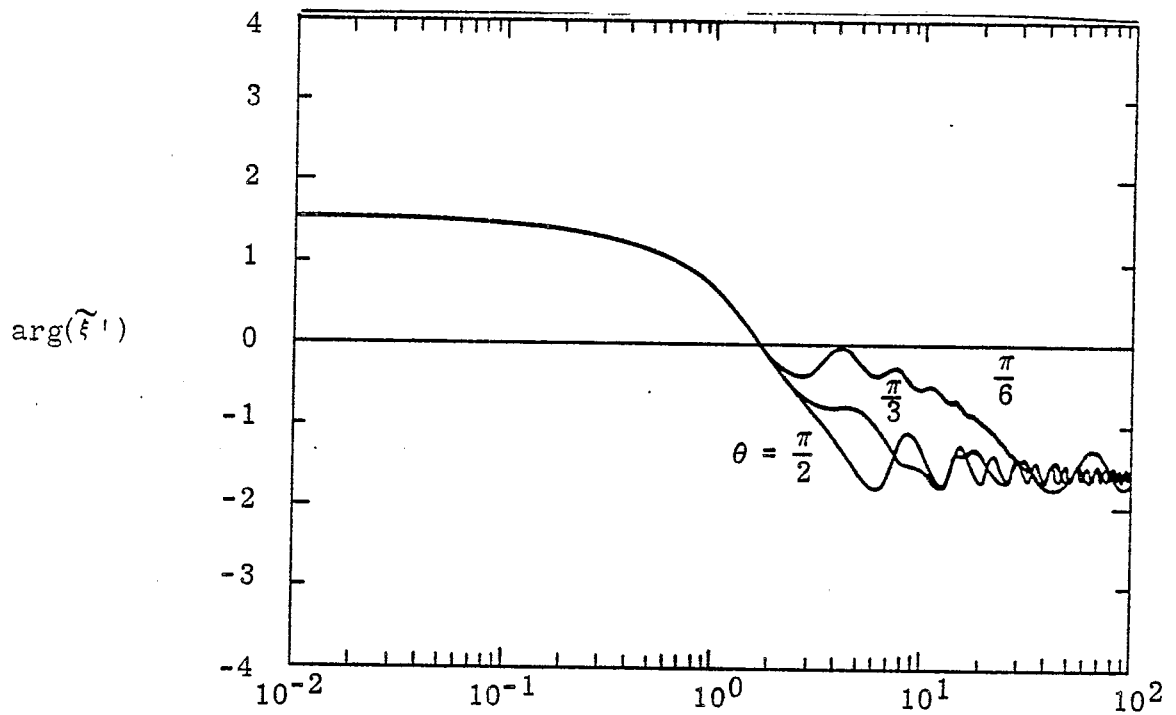


Figure 22b. Phase of $\tilde{\xi}'$ for $\theta = \frac{\pi}{2}, \frac{\pi}{3}, \frac{\pi}{6}$ with $\delta = 0.6$

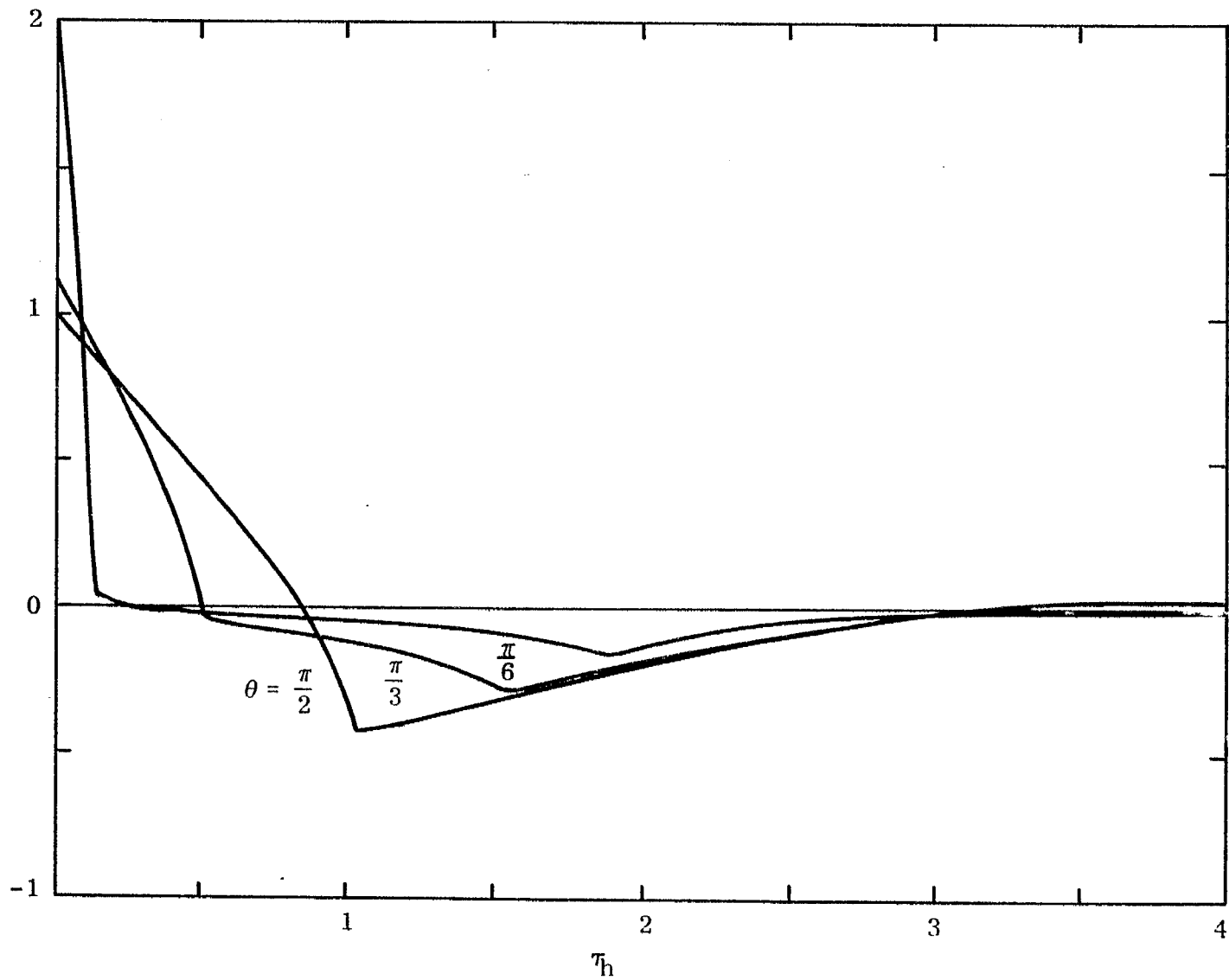


Figure 23. ξ' for $\theta = \frac{\pi}{2}, \frac{\pi}{3}, \frac{\pi}{6}$ with $\delta = 0.6$

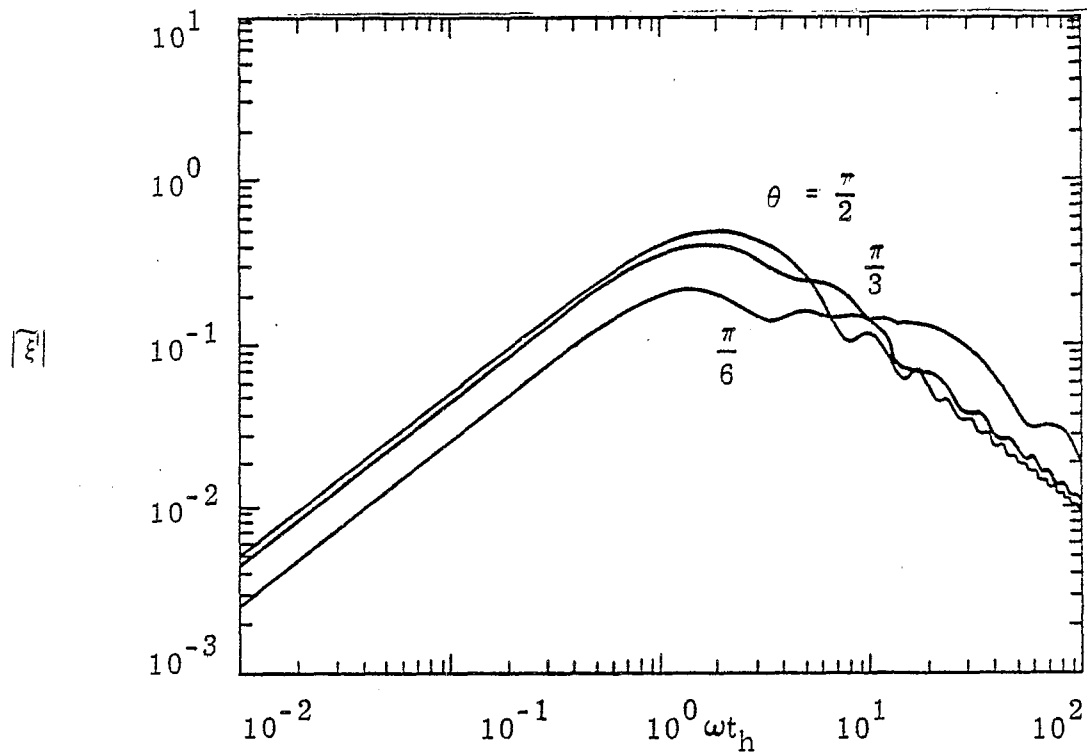


Figure 24a $|\tilde{\xi}|$ for $\theta = \frac{\pi}{2}, \frac{\pi}{3}, \frac{\pi}{6}$ with $\delta = 0.8$

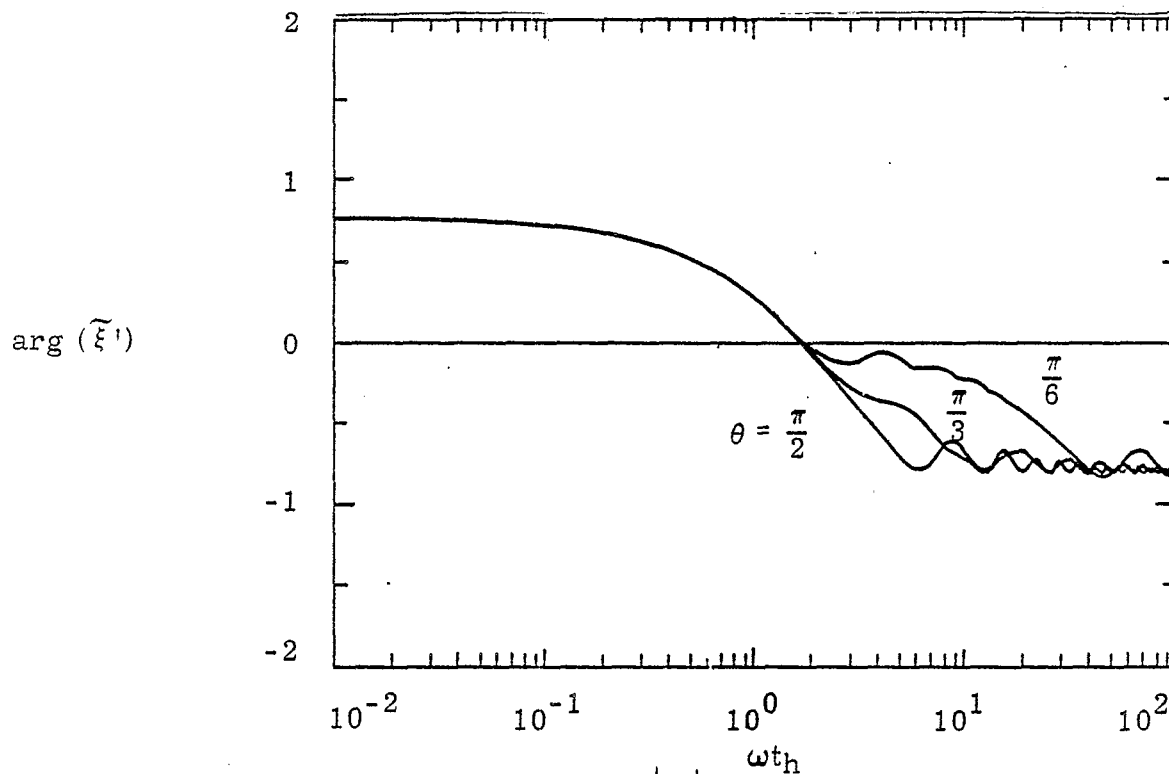


Figure 24b Phase of $|\tilde{\xi}'|$ for $\theta = \frac{\pi}{2}, \frac{\pi}{3}, \frac{\pi}{6}$, with $\delta = 0.8$

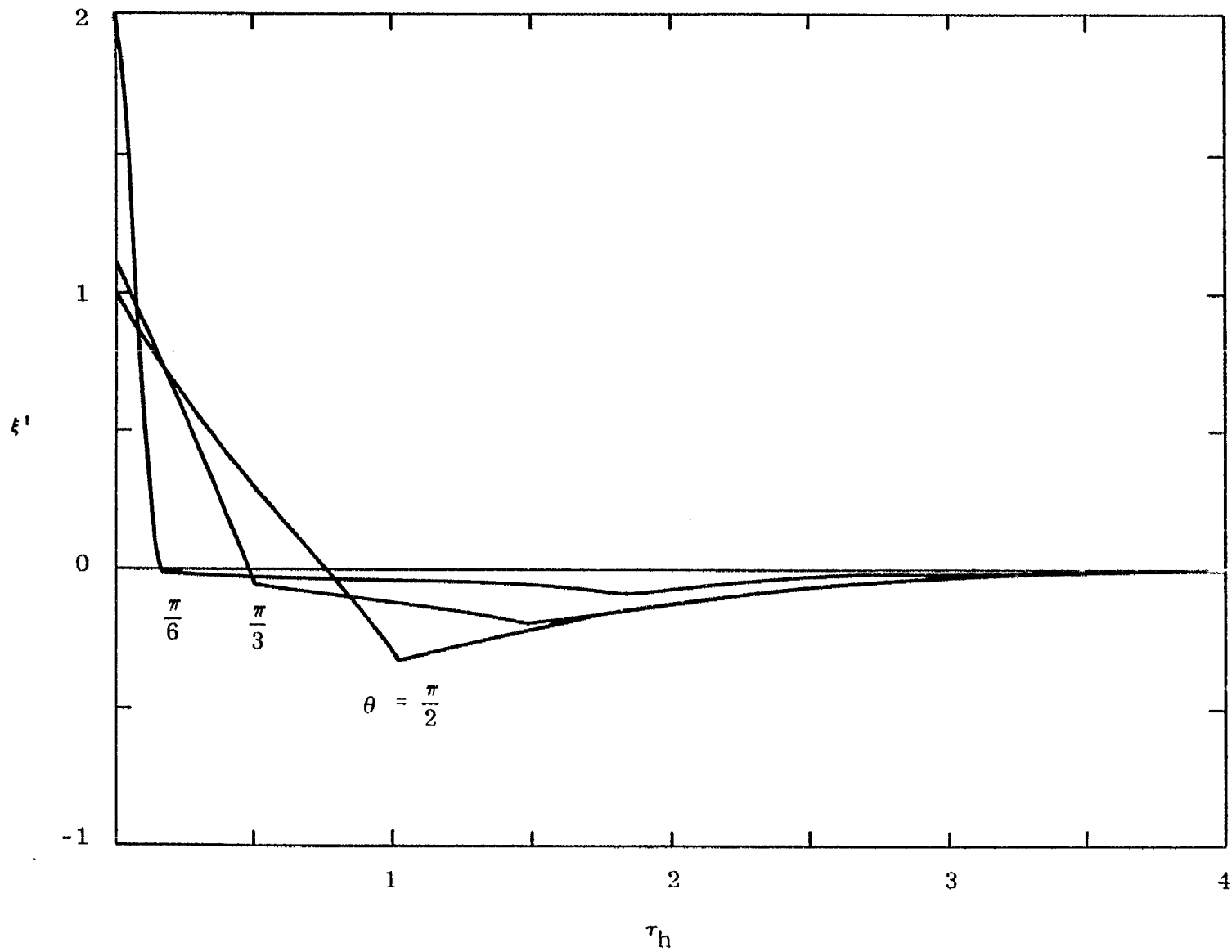


Figure 25 ξ' for $\theta = \frac{\pi}{2}, \frac{\pi}{3}, \frac{\pi}{6}$ with $\delta = 0.8$

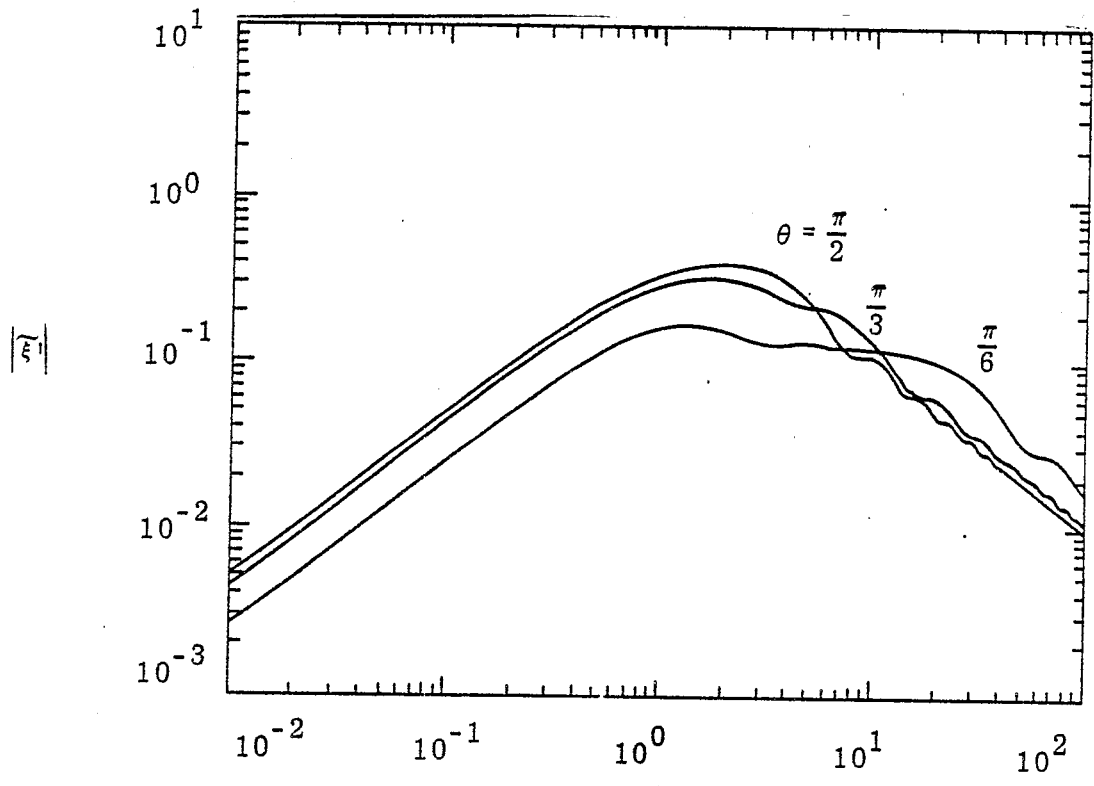


Figure 26a $|\tilde{\xi}'|$ for $\theta = \frac{\pi}{2}, \frac{\pi}{3}, \frac{\pi}{6}$ with $\delta = 1.0$

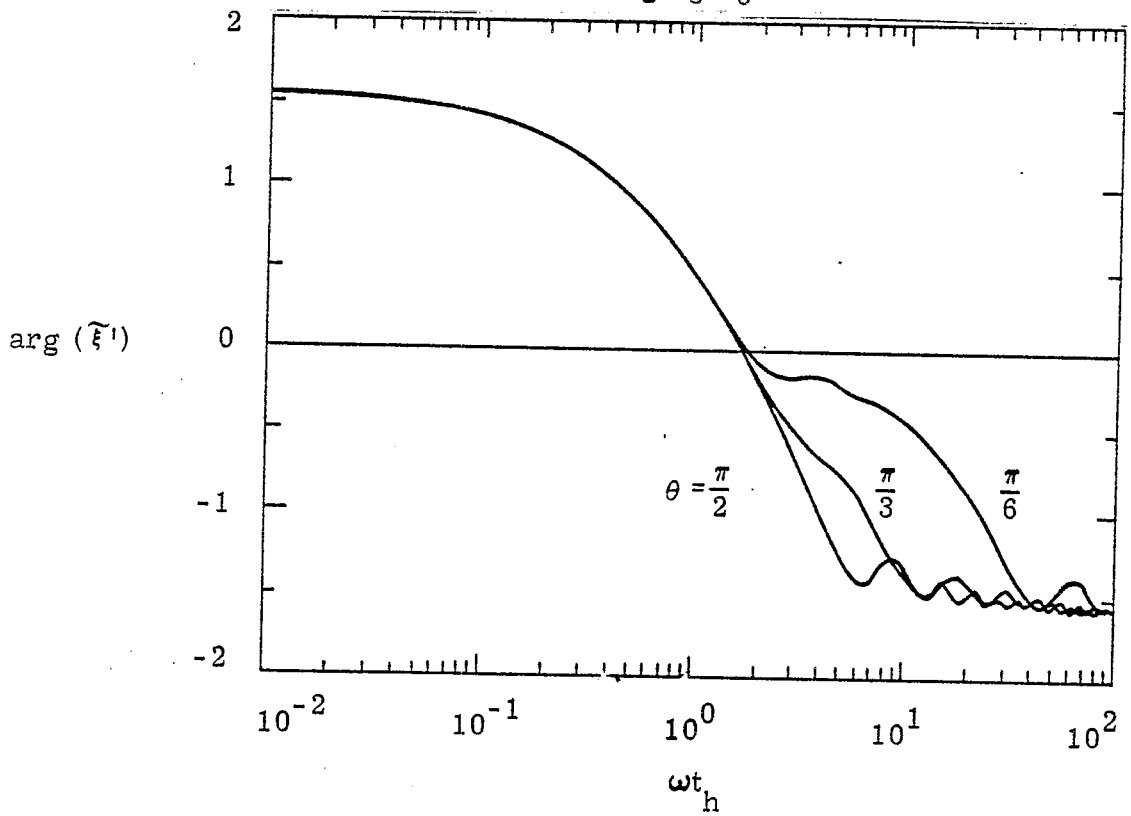


Figure 26b Phase ξ' for $\theta = \frac{\pi}{2}, \frac{\pi}{3}, \frac{\pi}{6}$ with $\delta = 1.0$

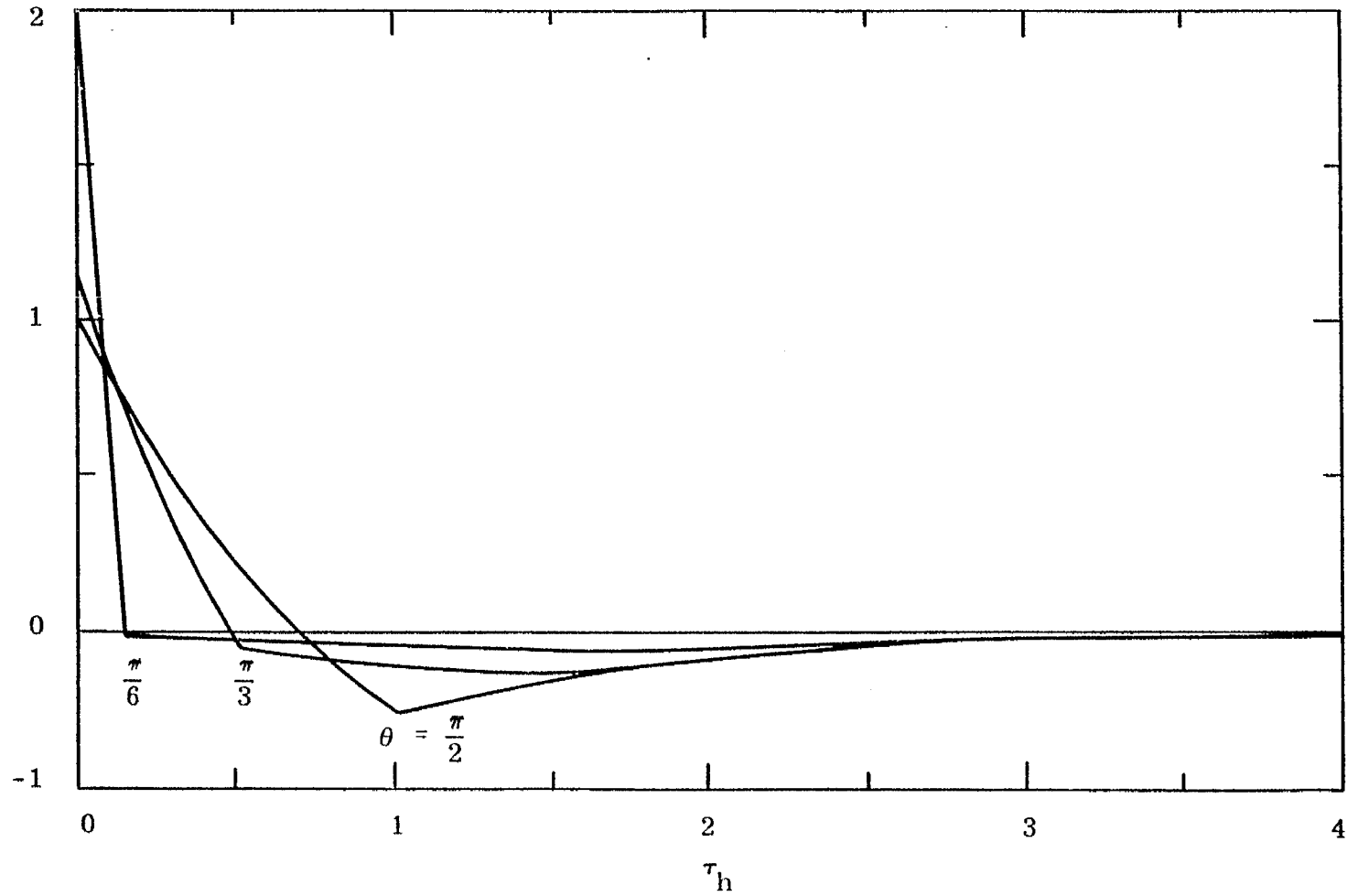


Figure 27 ξ' for $\theta = \frac{\pi}{2}, \frac{\pi}{3}, \frac{\pi}{6}$ with $\delta = 1.0$

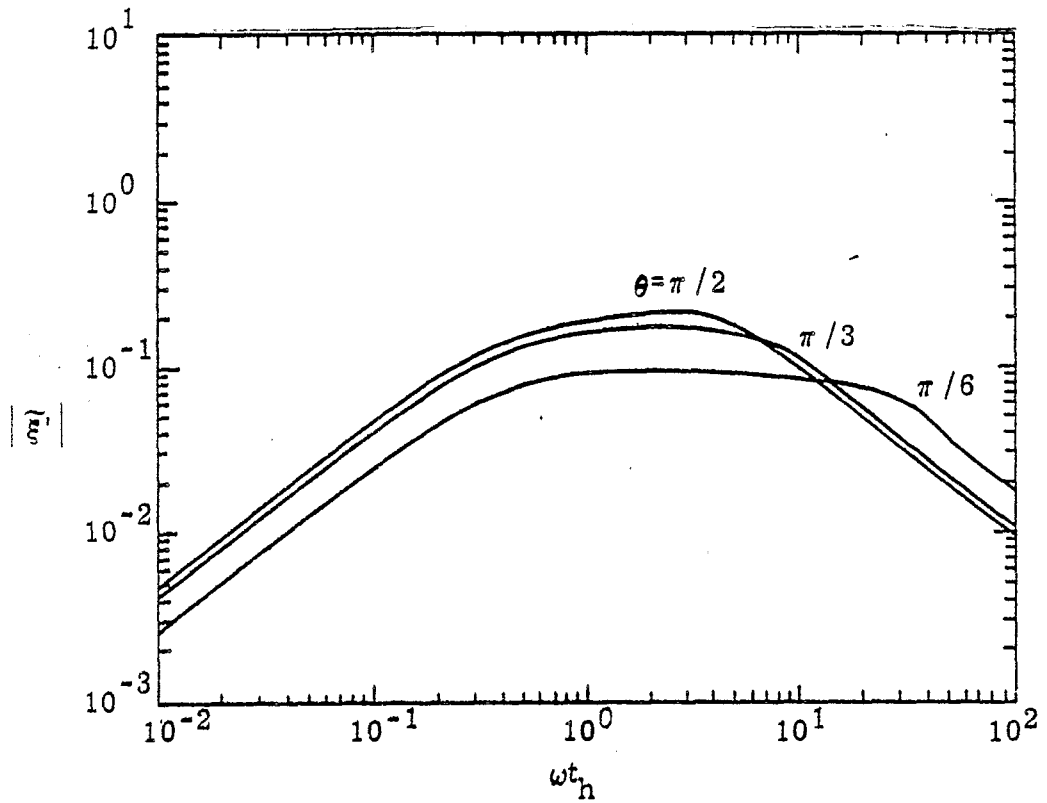


Figure 28a. $|\tilde{\xi}'|$ for $\theta = \pi/2, \pi/3, \pi/6$ with $\delta = 2.0$

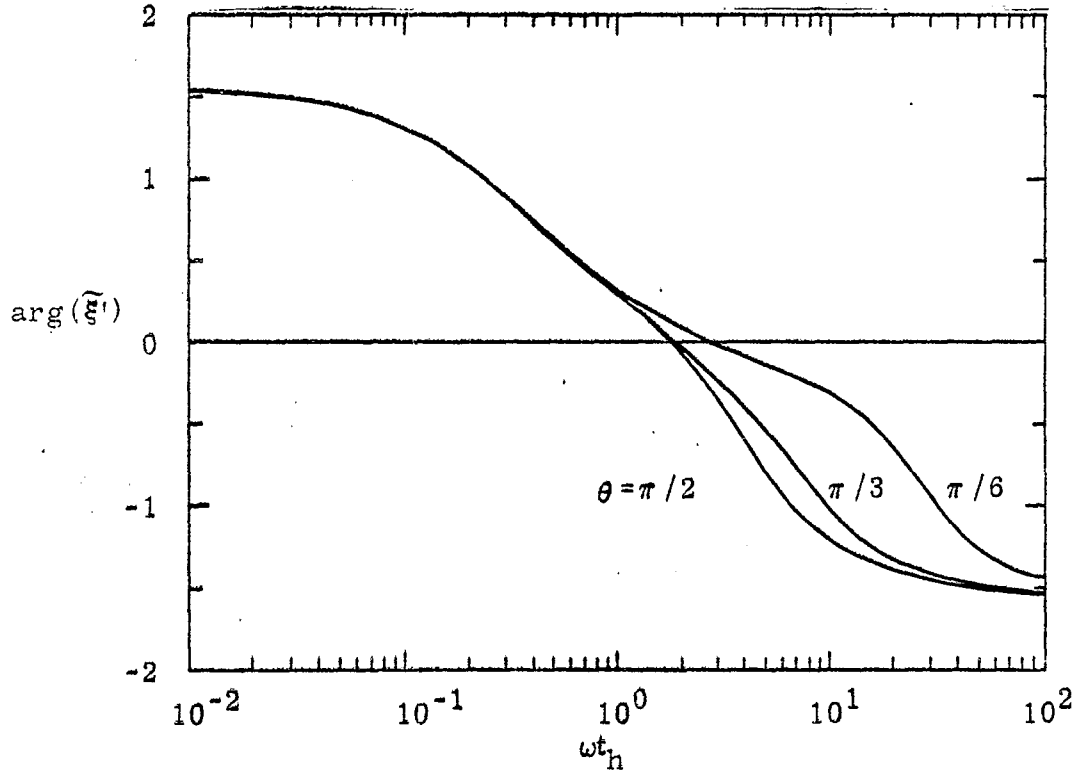


Figure 28b. Phase of $\tilde{\xi}'$ for $\theta = \pi/2, \pi/3, \pi/6$ with $\delta = 2.0$

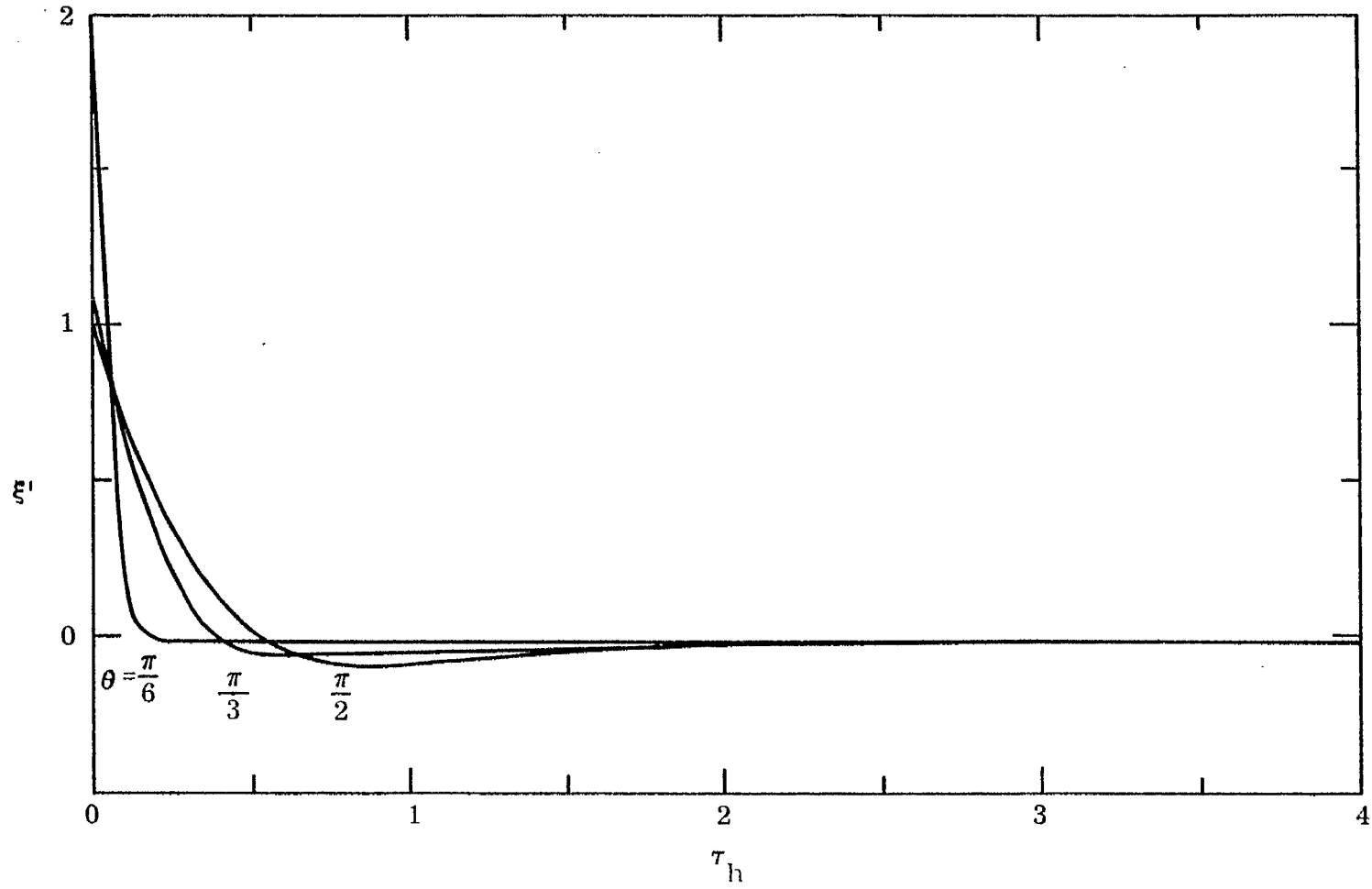


Figure 29. ξ' for Various $\theta = \frac{\pi}{2}, \frac{\pi}{3}, \frac{\pi}{6}$ with $\delta = 2$

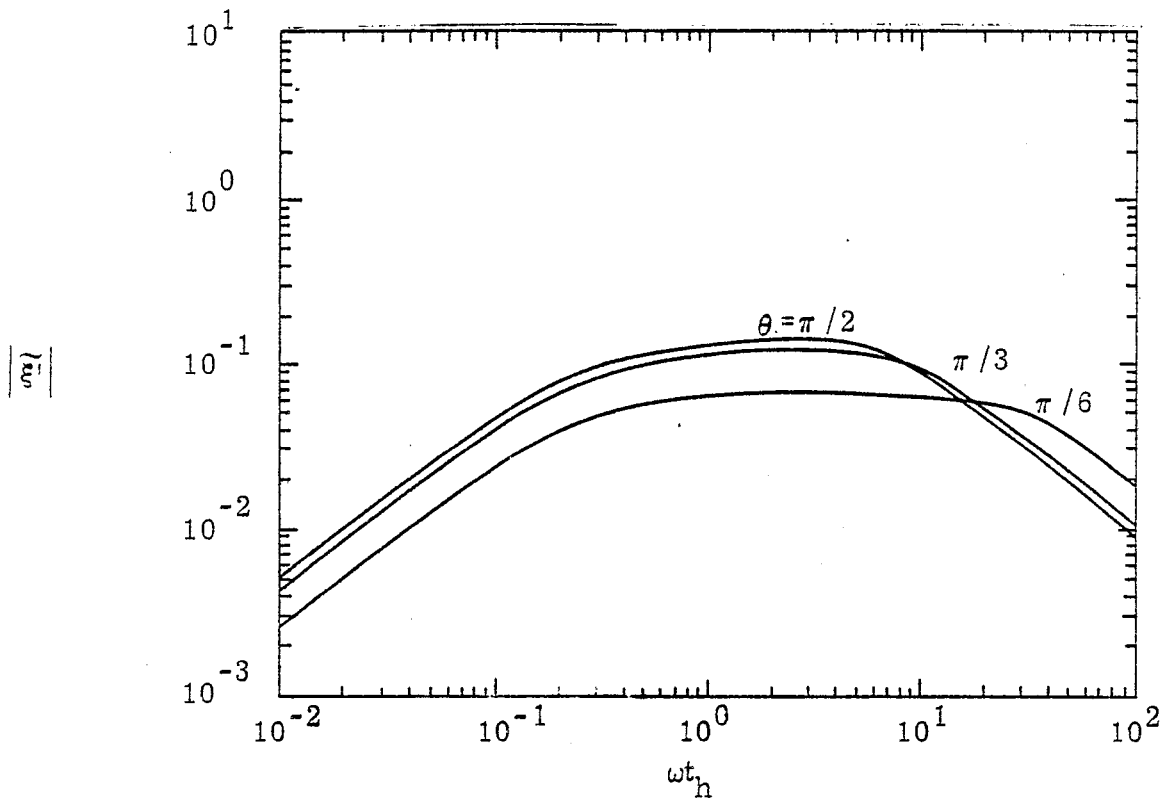


Figure 30a. $|\tilde{\xi}'|$ for $\theta = \pi/2, \pi/3, \pi/6$ with $\delta = 3.0$

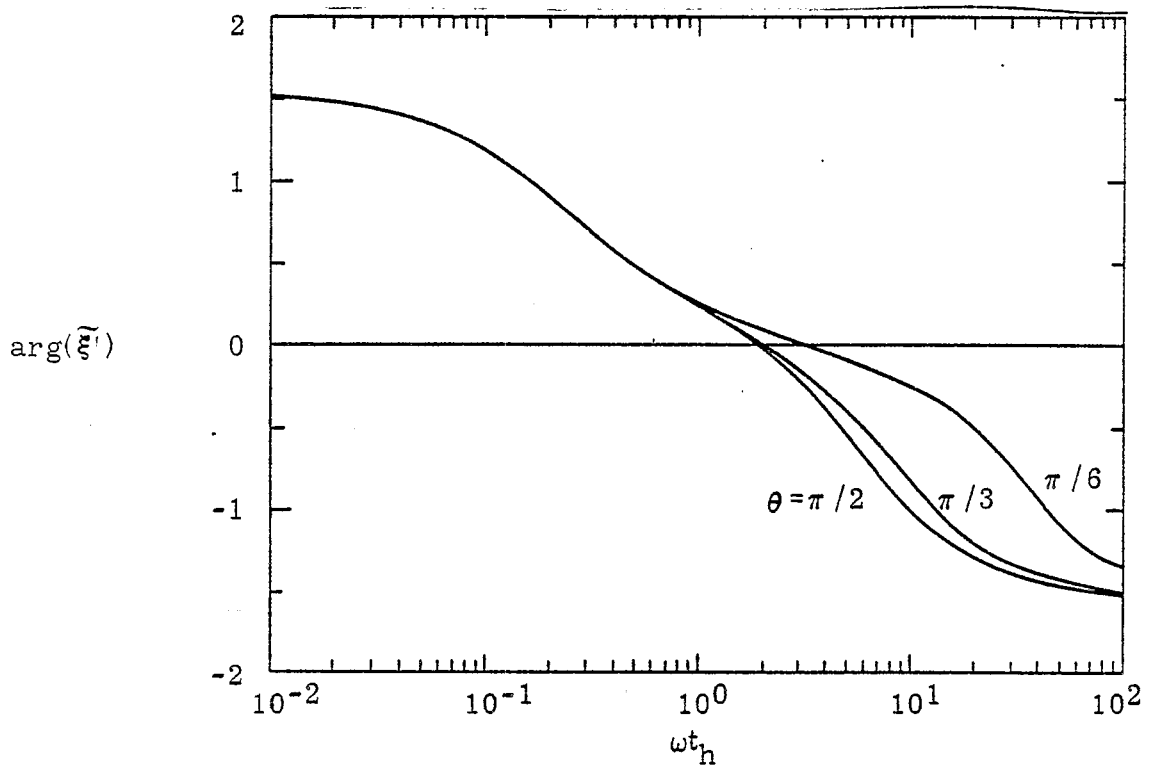


Figure 30b. Phase of $\tilde{\xi}'$ for $\theta = \pi/2, \pi/3, \pi/6$ with $\delta = 3.0$

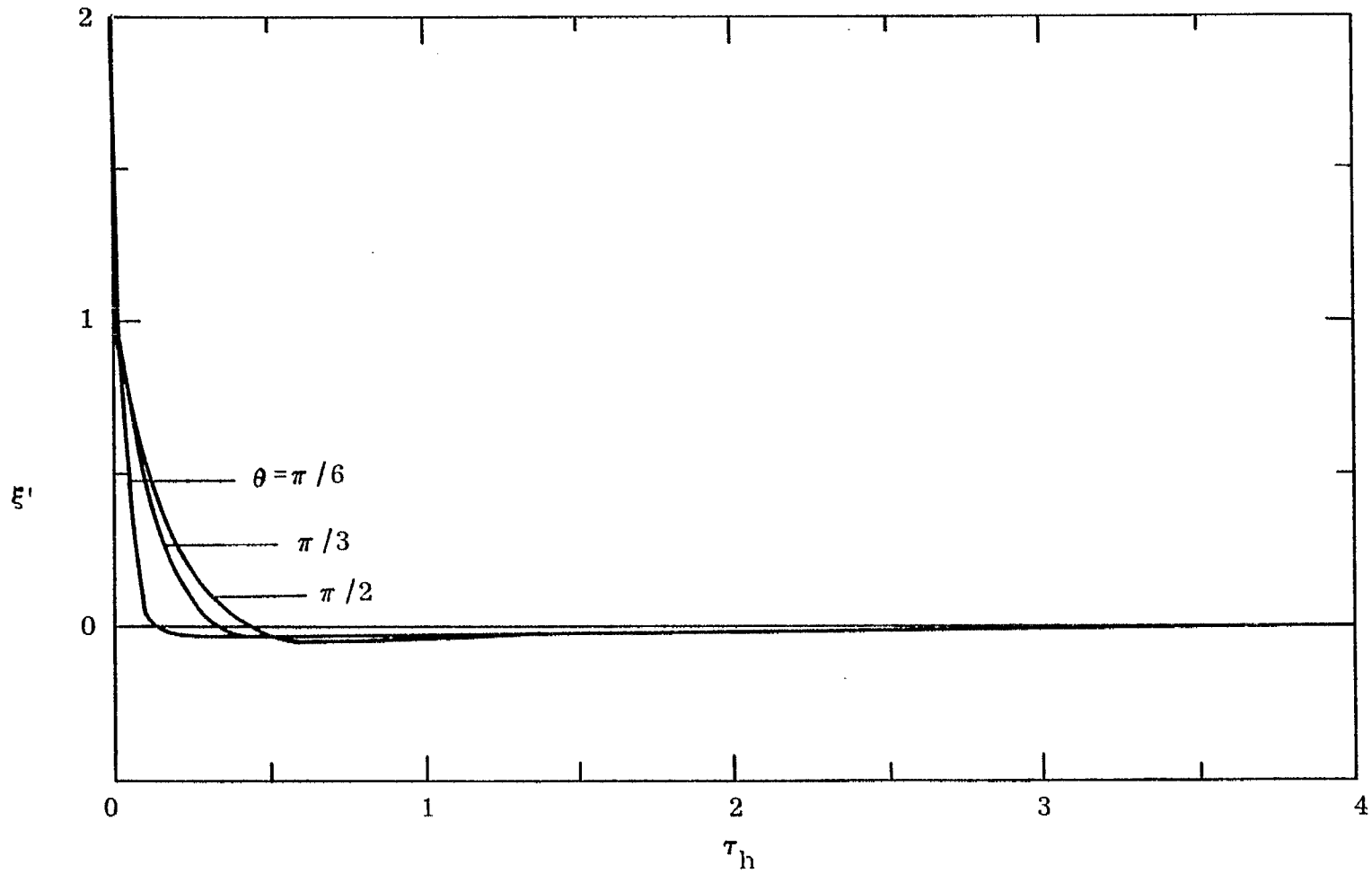


Figure 31. ξ' for $\theta = \pi/2, \pi/3, \pi/6$ with $\delta = 3.0$

in parallel with a resistance per unit length

$$R' = \frac{2 Z_{\infty}}{h - |z'|} \rho , \quad (58)$$

such that the total impedance per unit length is given by equation 3,

$$Z' = \frac{2 Z_{\infty}}{h - |z'|} \delta ,$$

then δ is related to ρ and λ by

$$\delta = \frac{s_h \lambda \rho}{s_h \lambda + \rho} \quad (59)$$

In order to separate δ into its real and imaginary parts, we set the variable

$$s_h = j\omega t_h$$

so that δ becomes

$$\begin{aligned} \delta &= \frac{j\omega t_h \lambda \rho}{j\omega t_h + \rho} \\ &= \frac{\rho(1 + j\rho/\omega t_h \lambda)}{1 + (\rho/\omega t_h \lambda)^2} \end{aligned} \quad (60)$$

Notice that in the high frequency limit,

$$\lim_{\omega \rightarrow \infty} \delta = \rho ,$$

and the impedance Z' appears purely resistive. In the low frequency limit

$$\lim_{\omega \rightarrow 0} \delta = \lim_{\omega \rightarrow 0} j\omega t_h \lambda = 0,$$

so that the antenna appears to be unloaded. The behavior of the real and imaginary components of δ/ρ as a function of $\lambda/\rho\omega t_h$ is shown in figure 32.

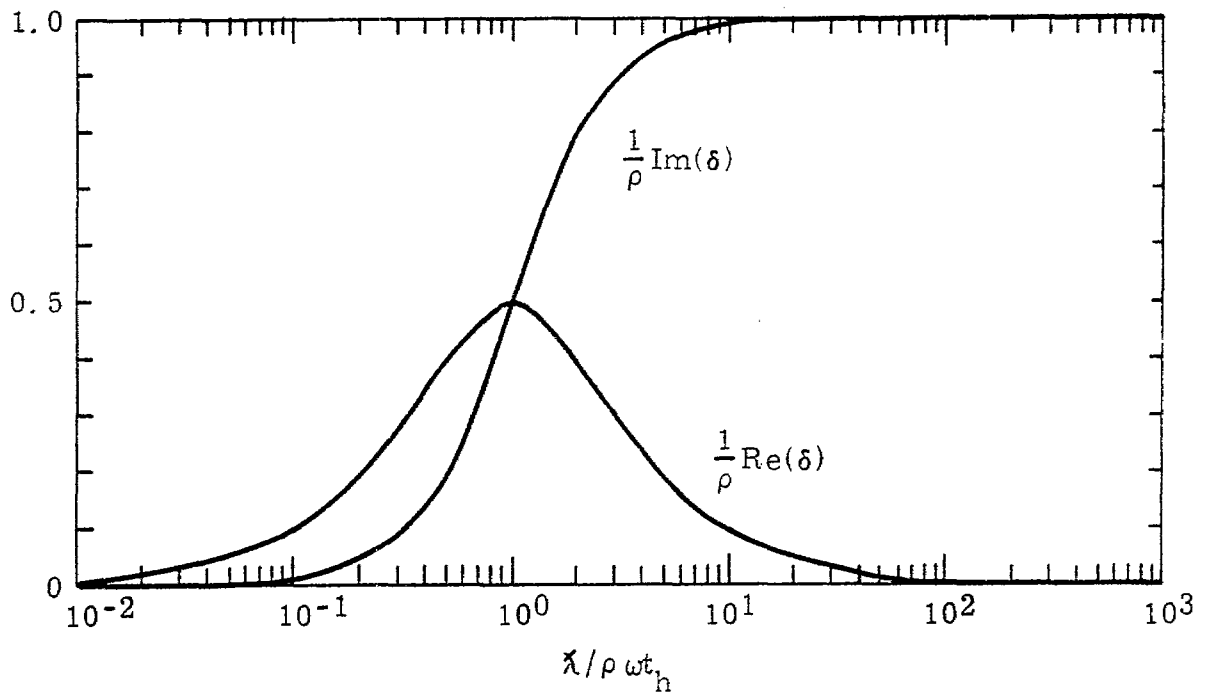


Figure 32. Behavior of $\frac{1}{\rho} \text{Re}(\delta)$ and $\frac{1}{\rho} \text{Im}(\delta)$ as a Function of $\lambda/\rho\omega t_h$

Figures 33 through 40 show some results of adding inductance in parallel with resistance. All these curves assume the observer is in the far field and at an angle $\theta = \frac{\pi}{2}$. Figures 33 through 38 are for a value of $\rho = 1$. Figures 39 and 40 are for $\rho = .5$. The loading parameter $\delta(s_h)$ is now given by

$$\delta(s_h) = \frac{s_h \rho \lambda}{s_h \lambda + \rho} \quad (60)$$

where ρ is the normalized resistance parameter and λ is the corresponding parallel inductance parameter.

It may be observed that the inclusion of parallel inductance significantly modifies the radiated wave in a number of respects. First, for $\rho = 1$, the first zero crossing time may be moved to values greater than $\tau_h = 1$. Secondly, the undershoot and second crossover time are affected. Also the discontinuity in slope at $\tau_h = 1$ is somewhat reduced and $\tau_h = 1$ is in general no longer the minimum point on the curve.

It may be remarked that even for relatively large parallel inductance, the value of ξ' for late times is affected by the inductance. For example, if $\lambda = 6$, $\rho = 1$, ξ' at $\tau_h = 4$ is larger by almost a factor of 2 than for the $\rho = 1$ case with $\lambda = \infty$.

The frequency domain results show filtering behavior with both the magnitude and the location of the peak of ξ' increased as λ is decreased. This highly resonant frequency domain behavior is reflected by the highly oscillatory behavior for the same cases in the time domain. Compare, for example, figures 33a and 34. As the inductive loading becomes large (large λ), the behavior approaches that of the purely resistively loaded case, as may be seen from both frequency and time domain data.

Attempts to analytically determine some kind of optimum choice of loading were unsuccessful. Instead, a few values of λ were selected for which the second zero crossing (for $\rho = 1$) had not yet occurred at

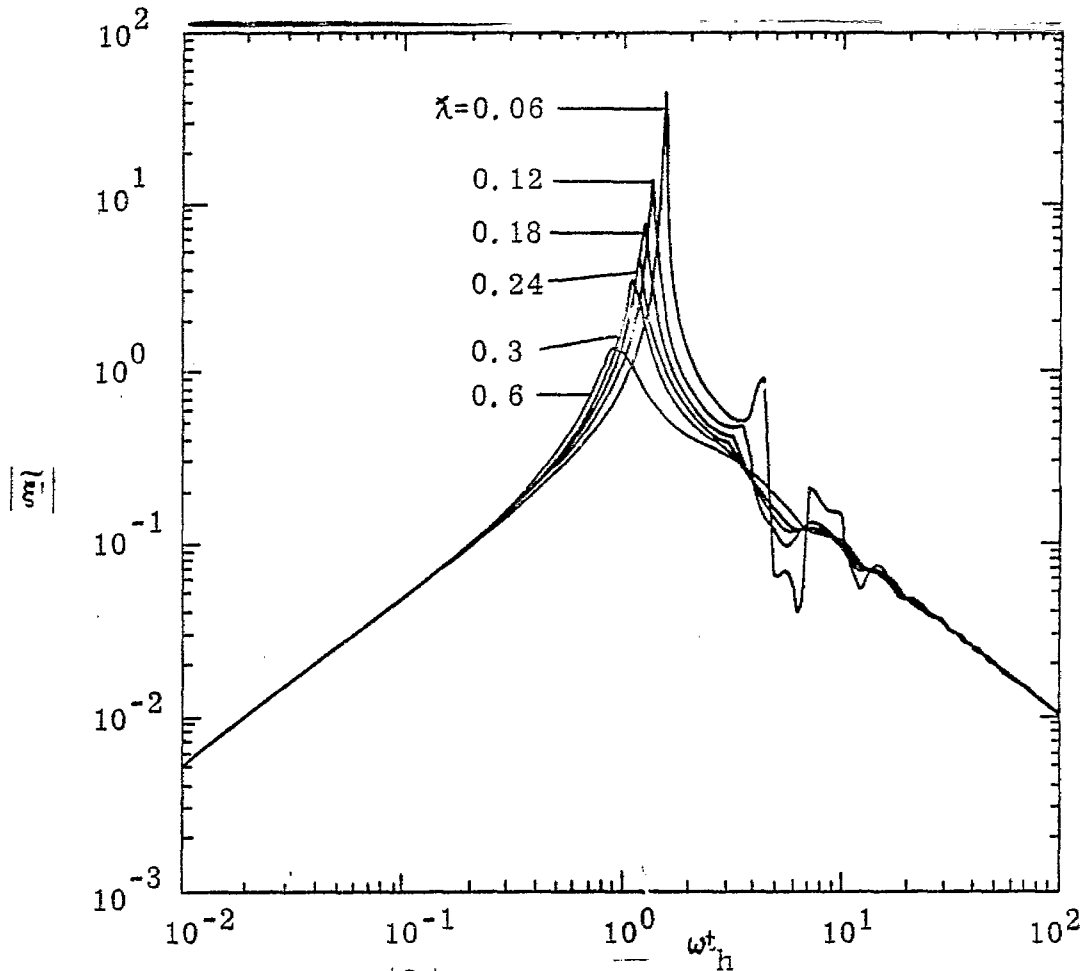


Figure 33a. $|\tilde{\xi}|$ for Various λ with $\rho = 1$

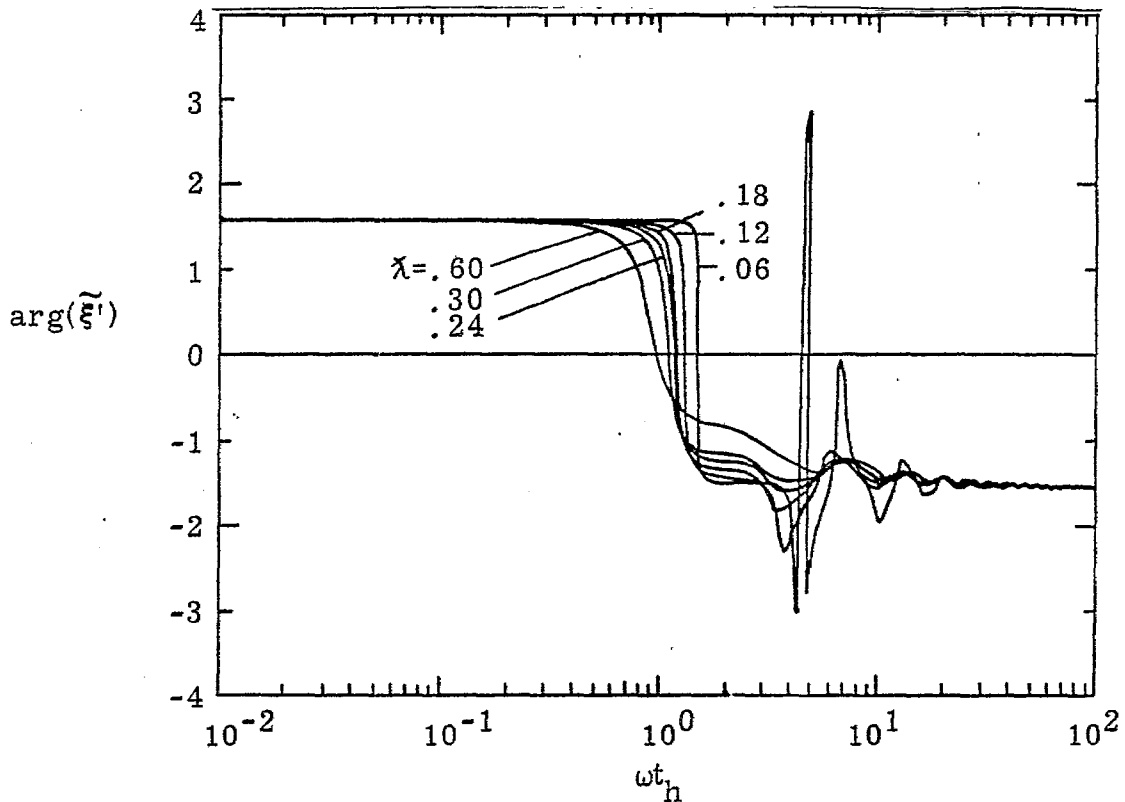


Figure 33b. Phase of $\tilde{\xi}$ for Various λ with $\rho = 1$

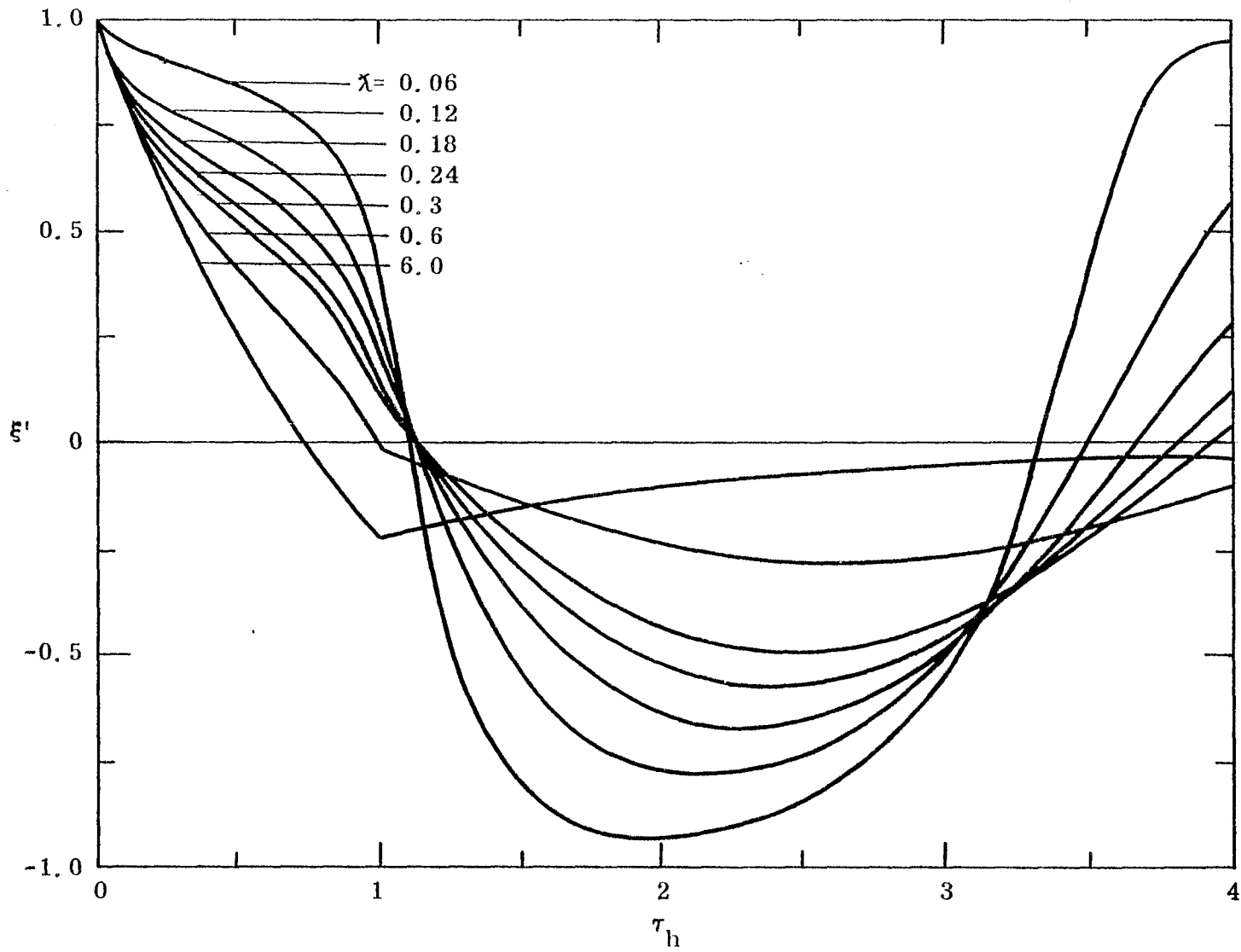


Figure 34. ξ' for Various λ with $\rho = 1$

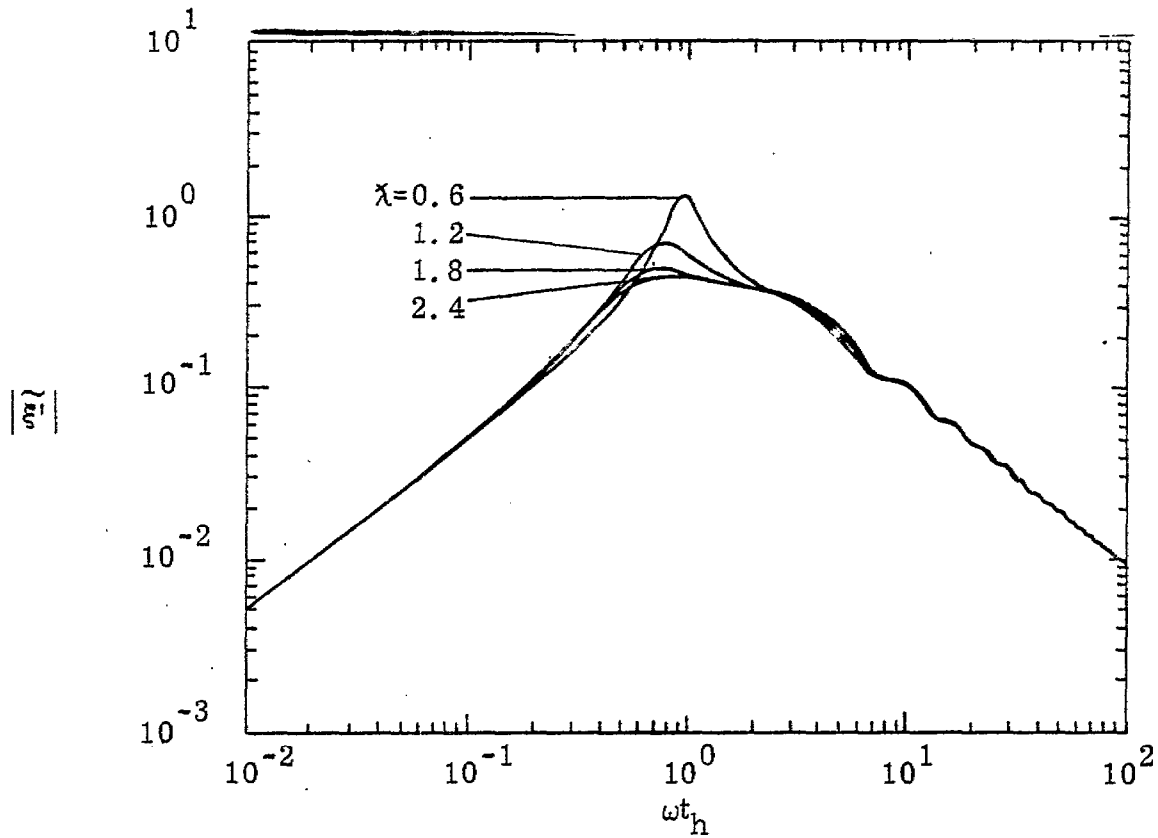


Figure 35a. $|\tilde{\xi}'|$ for $\lambda = .6, 1.2, 1.8, 2.4$ and $\rho = 1$

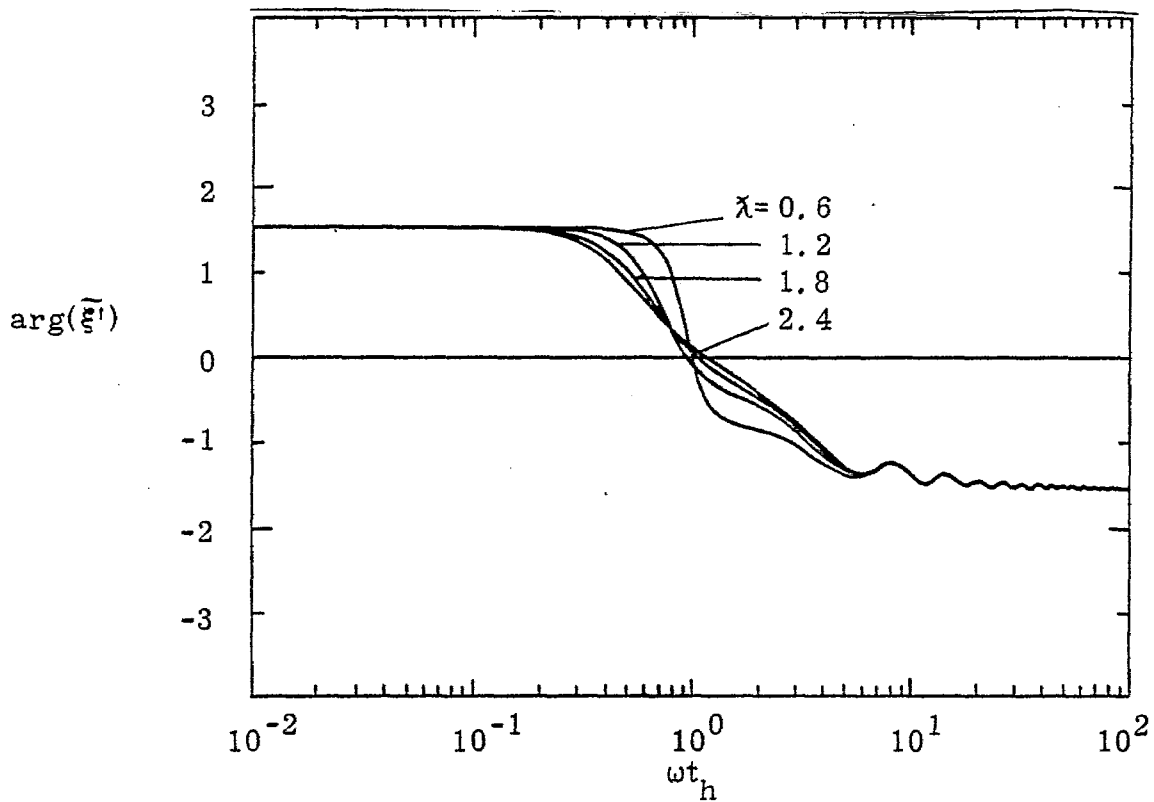


Figure 35b. Phase of $\tilde{\xi}'$ for $\lambda = 0.6, 1.2, 1.8, 2.4$ with $\rho = 1$

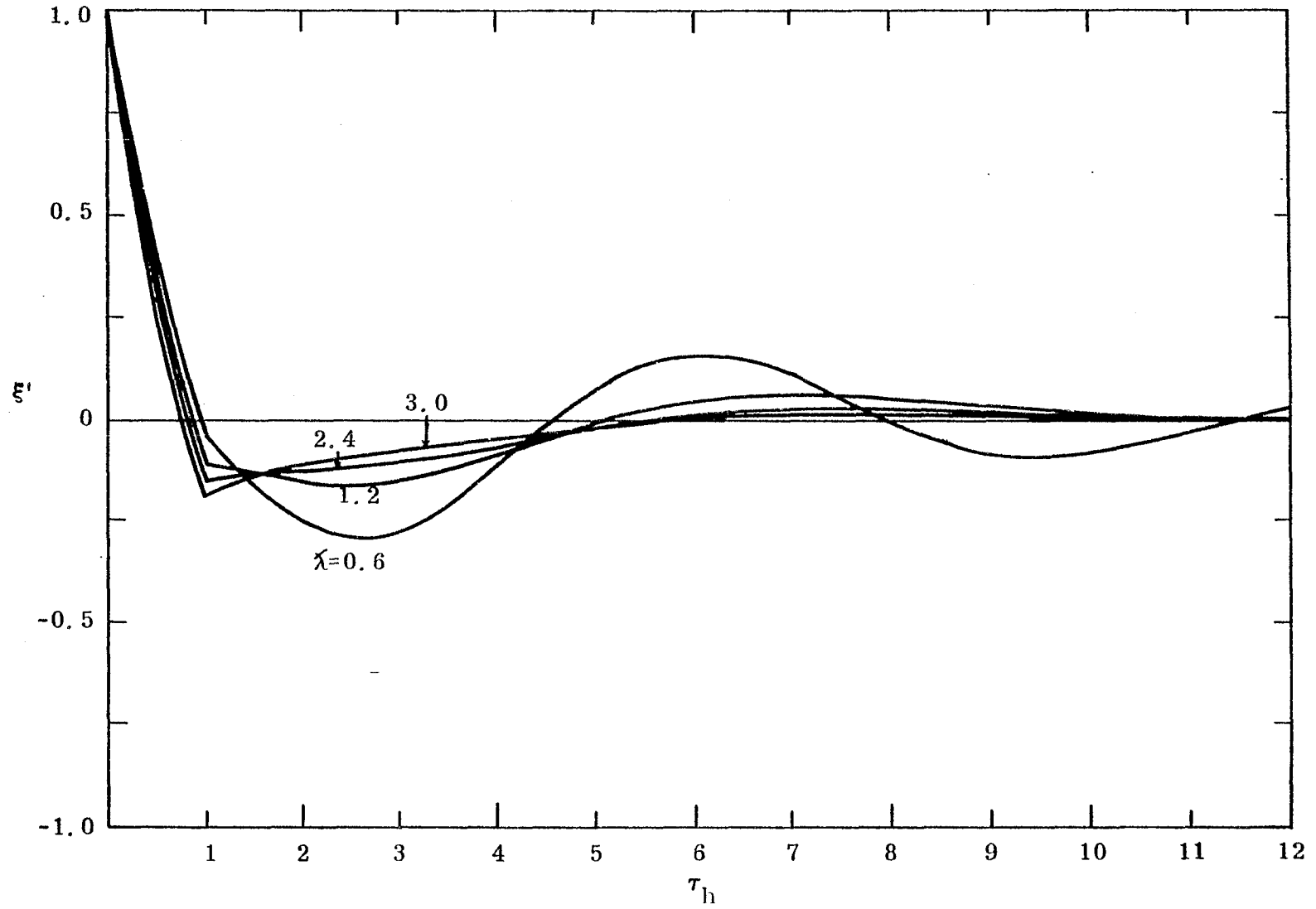


Figure 36. ξ' for Various λ with $\rho = 1$

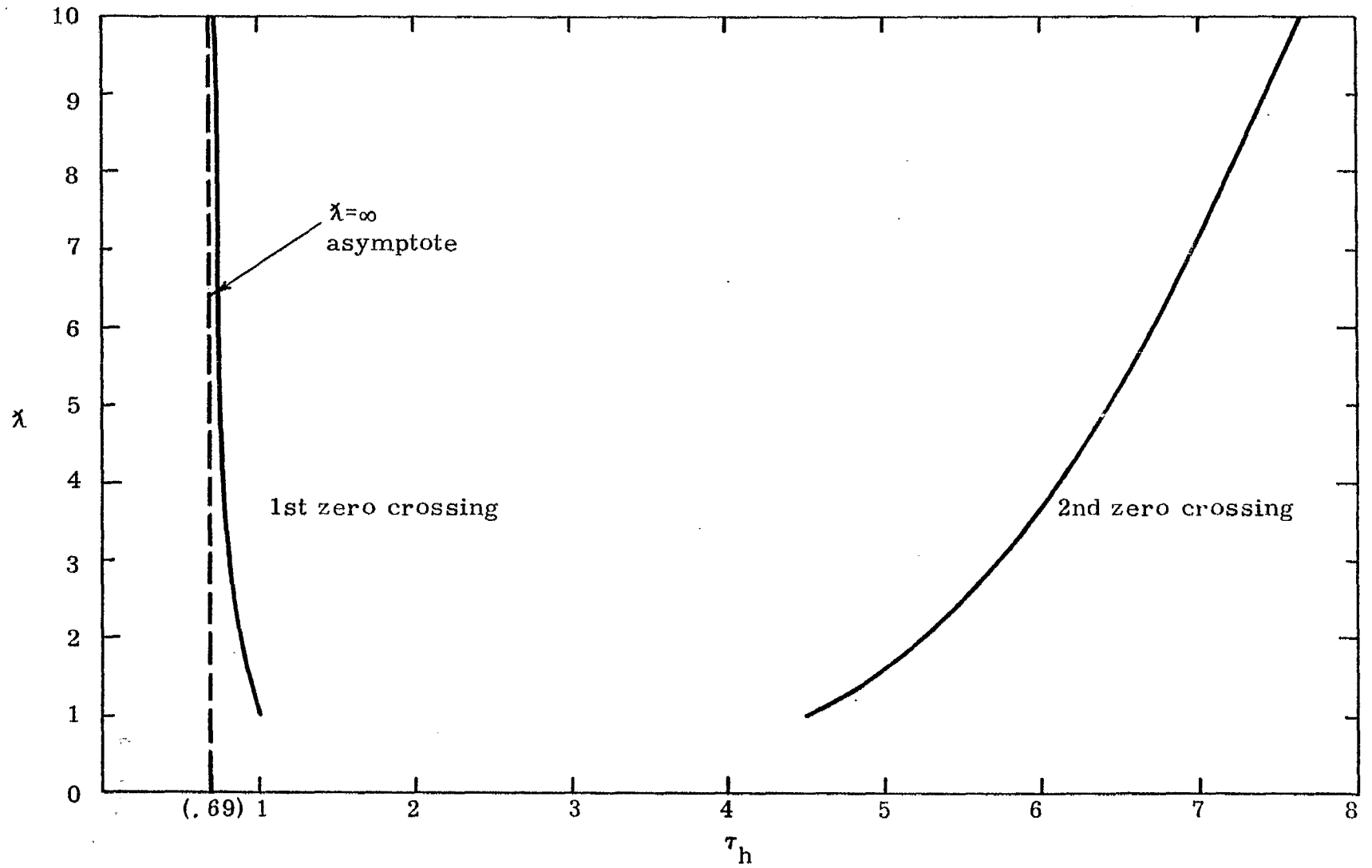


Figure 37. Variation of First and Second Zero Crossing Times with λ with $\rho = 1$

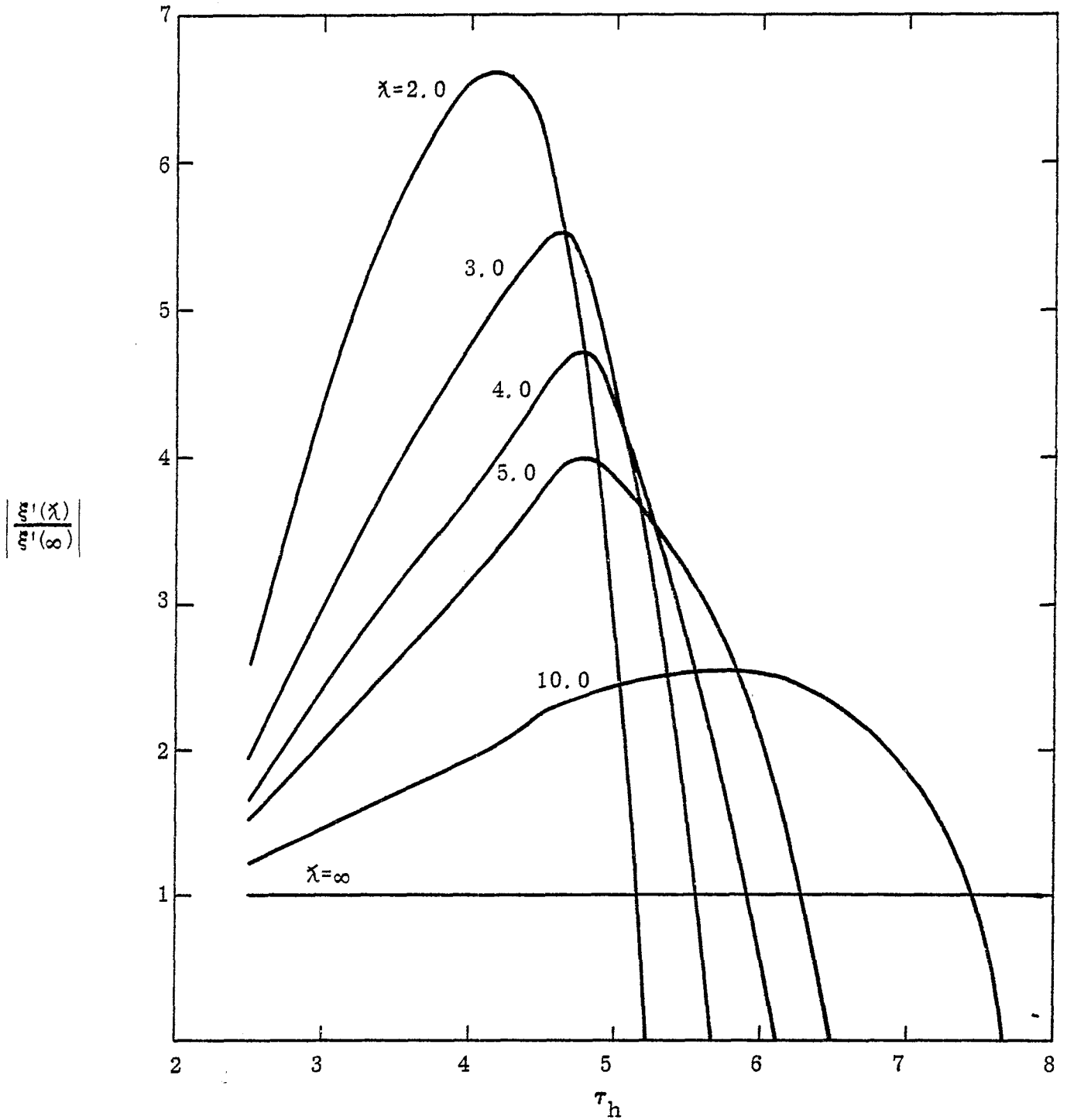


Figure 38. Relative Field Strength with χ as a Parameter

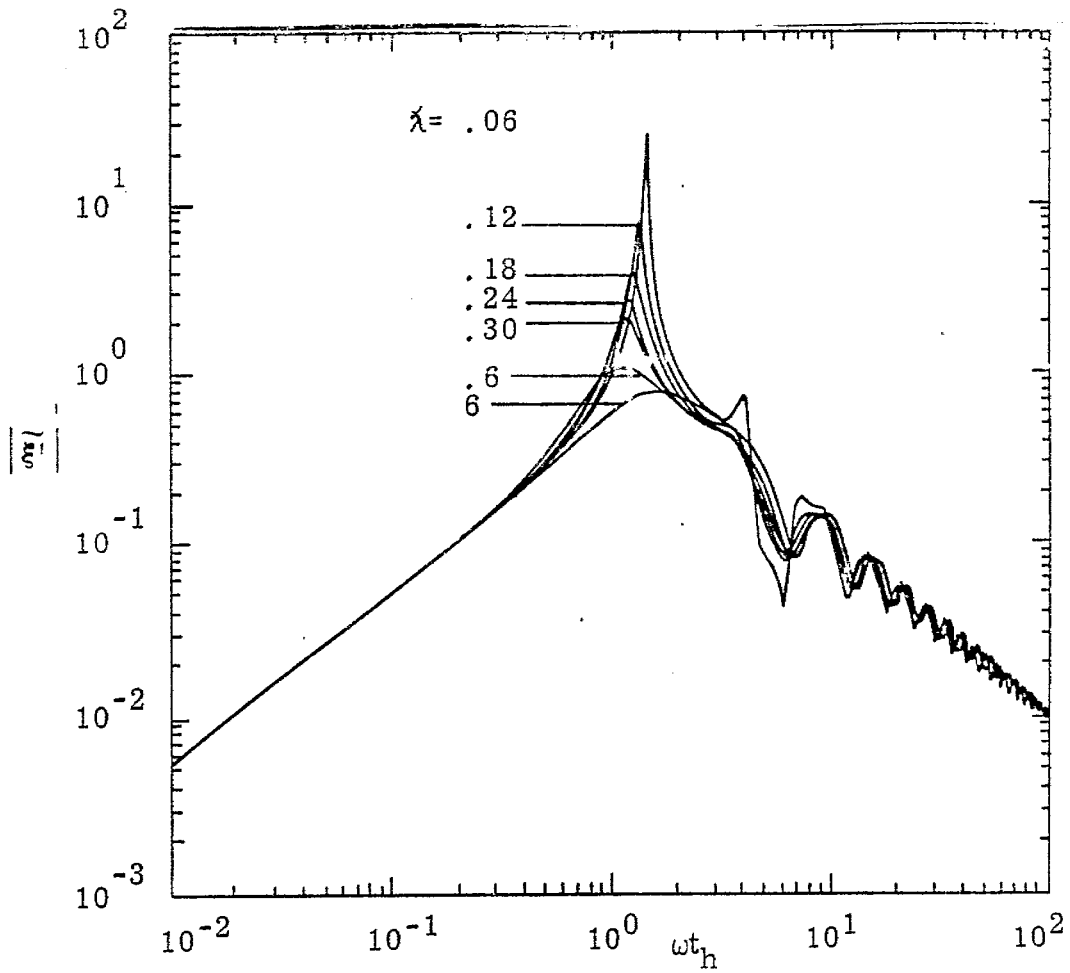


Figure 39a. $|\tilde{\xi}'|$ for Various λ with $\rho = .5$

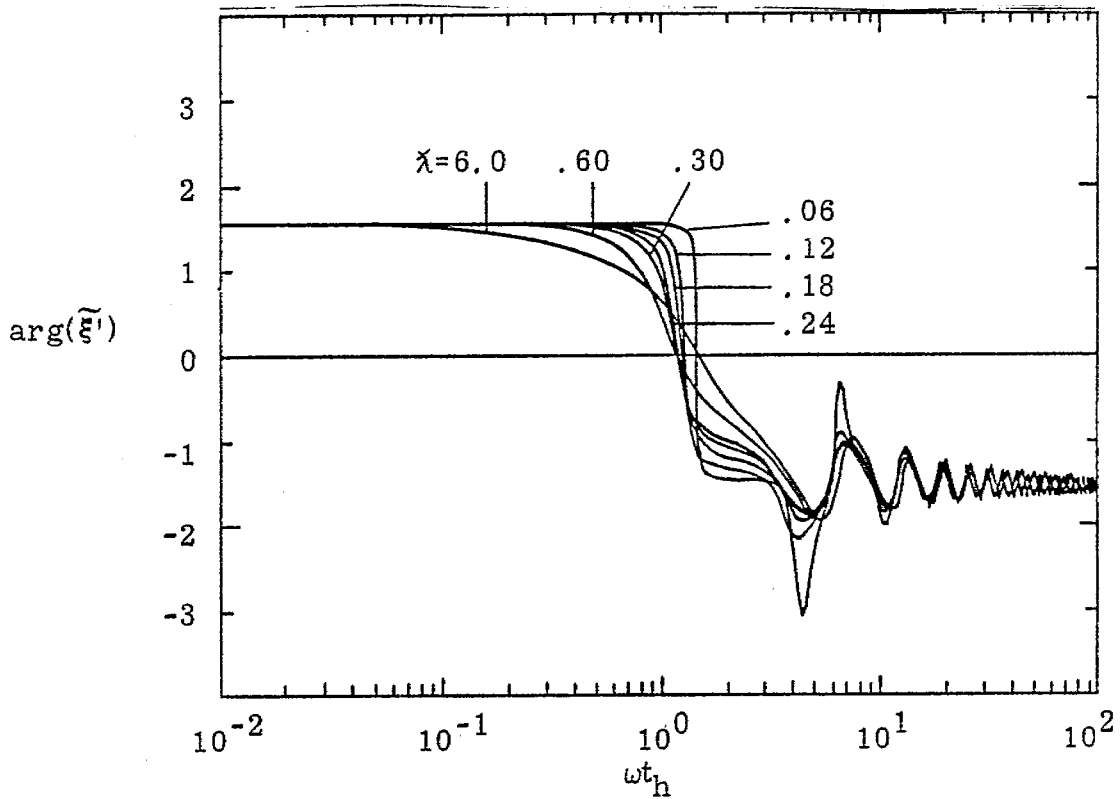


Figure 39b. Phase of $\tilde{\xi}'$ for Various λ with $\rho = .5$

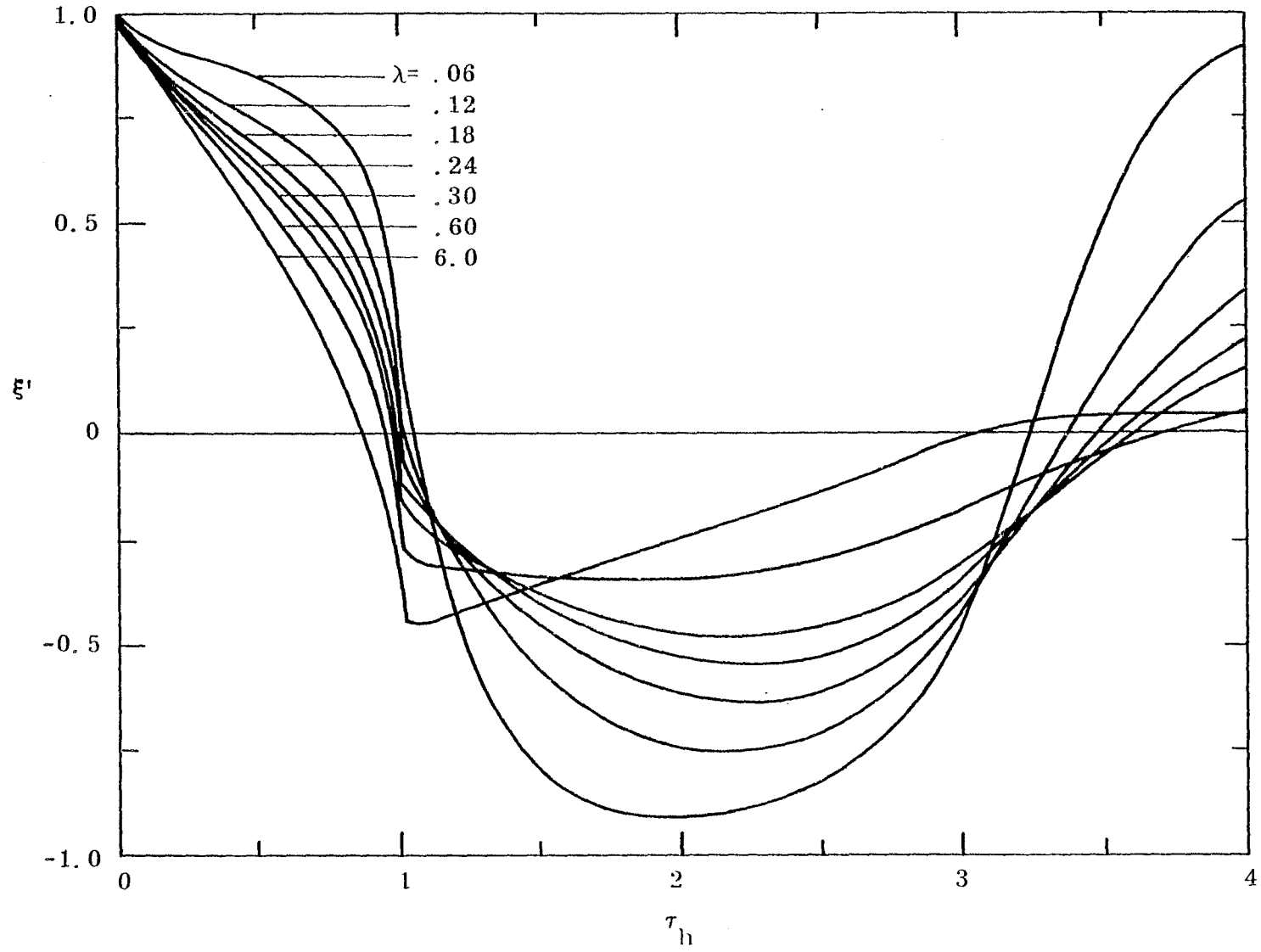


Figure 40. ξ' for Various λ with $\rho = .5$

$\tau_h = 4$. Time domain data were extended for these cases to $\tau_h = 12$ with the results shown in Figure 36. From figure 36 it may be concluded that the second zero crossing may be pushed to values exceeding $\tau_h = 6$. To further clarify the zero crossing question, figure 37 shows first and second zero crossing times as a function of λ with $\rho = 1$ assumed throughout. The $\rho = 1$ value is chosen since for pure resistive loading of $\rho = 1$, the second zero crossing is at infinity. Although not proven analytically, the numerical results suggest that $\rho = 1$ is the minimum value of ρ such that the second zero crossing is at infinity. For $\rho = 0.8$ there is a second zero crossing at $\tau_h \approx 4.5$, for example. Thus, $\rho = 1$, $\lambda = \infty$ provides a useful reference case against which to compare the $\rho = 1$, $\lambda \neq \infty$ cases. The numerical results suggest that for any finite λ there is a finite second zero crossing time, (at least if $\rho = 1$ is assumed) but that one may delay this time to any arbitrarily large value at the expense of field strength by selecting a large enough λ . Figure 38 shows the ratio of the radiated electric field for various inductively loaded cases to the electric field radiated by an antenna purely resistively loaded with $\rho = 1$ for all cases. The times shown are between the first and second zero crossing times for each case. The ratios may be viewed as a measure of the improvement in field strength due to the resistive-inductive loading as compared to the purely resistively loaded case for the times shown.

The conclusion is that if a second zero crossing at some finite time is acceptable, the addition of parallel inductance will increase the late time fields by an amount dependent on the second zero crossing time. Figures 39 and 40 are similar to figures 33 and 34, but with $\rho = .5$ instead of 1. The behavior is quite similar in the two cases.

The accuracy of the numerical results depends upon two things: (1) The calculation of the confluent hypergeometric function appearing in equation 28, and (2) the number of frequency points used in the transformation from the frequency to the time domain. The confluent hypergeometric function is calculated by a power series in the argument

$-2\gamma_0 (h-|z'|)$, and for large argument by an asymptotic expansion in $-2\gamma_0 (h-|z'|)$. The number of terms in either series together with the number of frequency points required are chosen such that the time domain function ξ' agrees to within at least 1% with the analytical results at $\tau_h = 0$ for the case of purely resistive loading.

VIII. Application

In order to illustrate the impact of the above calculations on real antenna systems, we consider the application of these results to a specific antenna. We choose the following specifications:

Antenna half-length - $h = 50$ meters

Effective antenna cage radius - $a = 2.5$ meters

Peak source voltage (assuming capacitive generator) - $V_o = 5 \times 10^6$ volts

From equation 2, above we calculate the characteristic impedance of this antenna as

$$Z_\infty = \frac{Z_o}{\pi} \ln 40 = 442 \Omega$$

so that $f_g = Z_\infty / Z_o = 1.17$

The relation between the far electric field and the normalized waveform is, from equation 27,

$$E_{f_\theta} = \frac{V_o}{2\pi f_g r} \xi'$$

For this antenna,

$$E_{f_\theta} = 6.78 \times 10^5 \frac{\xi'}{r}$$

An observer a distance 500 meters from the antenna experiences an electric field

$$E_{f_\theta} = 1.36 \times 10^3 \xi' \text{ volts/meter}$$

The retarded time for this observer (time measured from pulse onset) is related to the normalized time, τ_h , by

$$\begin{aligned} t^* &= \frac{h\tau_h}{c} \\ &= \frac{5000}{3} \tau_h \text{ nanoseconds} \end{aligned}$$

Choosing the impedance loading such that $\rho = 1$, $\chi = 6$, we obtain an inductive loading

$$L = \frac{L'}{2} = 442 \frac{1}{h-|z'|} \mu\text{H/meter}$$

in parallel with a resistive loading

$$R = \frac{R'}{2} = 442 \frac{1}{h-|z'|} \Omega/\text{meter}.$$

We can approximate this continuous loading by discrete loading elements. To obtain a bound on the required values of these discrete inductor and resistor elements, we assume the antenna to be loaded at 5 meter intervals. The largest values of both inductance and resistance will be required for the elements nearest the end of the antenna, which we take to be 45 meters from the antenna center. The required resistance at this location is taken to be

$$\begin{aligned} R &= \frac{R'}{2} = Z_\infty \int_{42.5}^{47.5} \frac{1}{50-z} dz \\ &= Z_\infty \ln \left(\frac{7.5}{2.5} \right) \end{aligned}$$

$$R = 486 \Omega$$

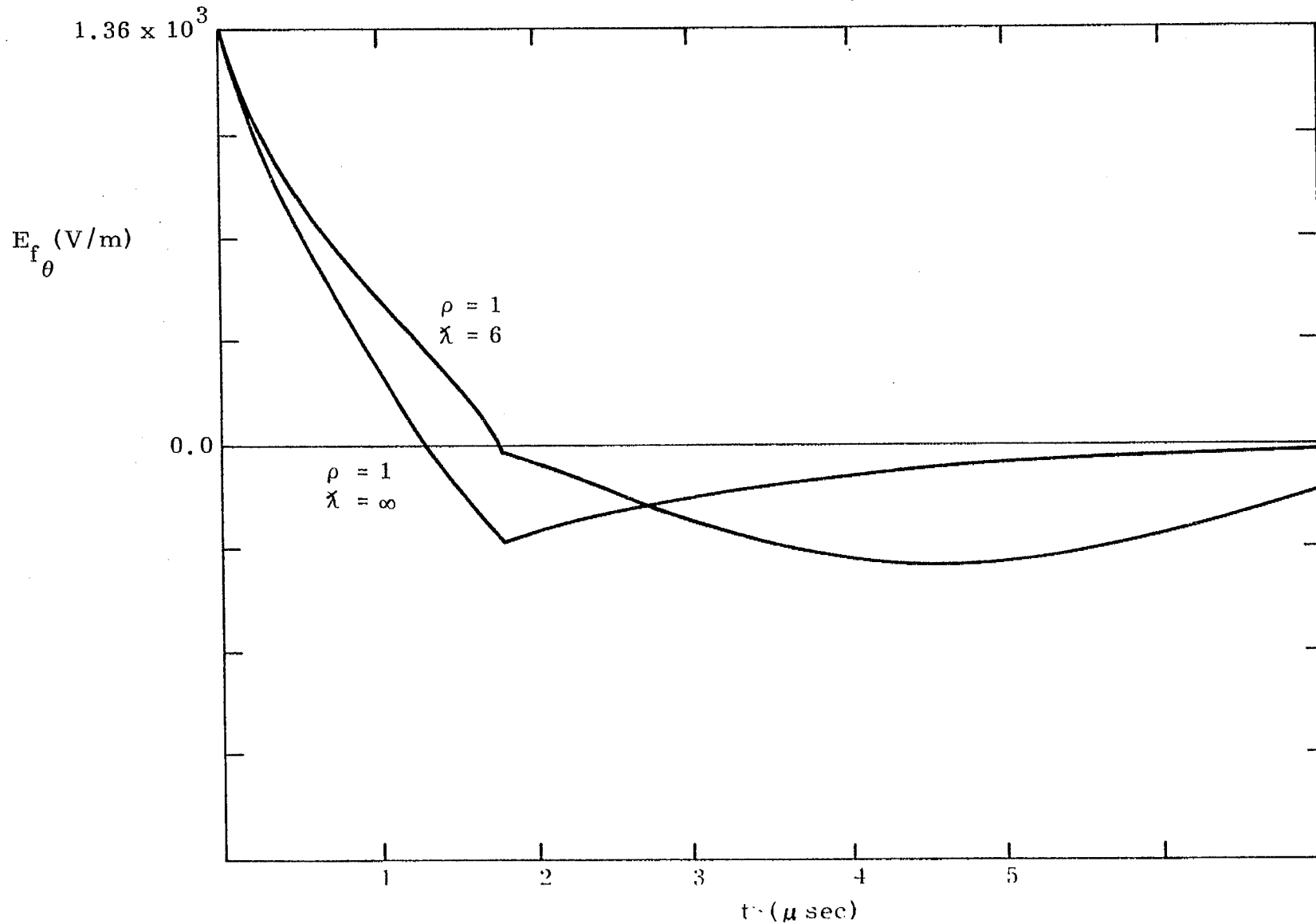


Figure 41. The Time Domain Far Electric Field Produced by Both Inductive and Resistive Loading ($\rho = 1$, $\chi = 6$), and by Resistive Loading Only ($\rho = 1$, $\chi = \infty$) Discussed in the Text

and the required inductance is taken as

$$L = \frac{L'}{2} = 10^{-6} Z \int_{42.5}^{47.5} \frac{1}{50-z} dz$$

$$L = 0.486 \mu\text{H}$$

The time domain electric field produced by this loading at $\theta = \pi/2$, $r = 500$ meters is shown in figure 41, together with that produced by only the resistive loading. Notice that the cross-over time with the inductive load included is approximately 500ns later than that with only resistive loading.

IX. References

1. D. E. Merewether, Sensor and Simulation Note 70, Transient Pulse Transmission Using Impedance Loaded Cylindrical Antennas, February 1968.
2. D. E. Merewether, Sensor and Simulation Note 71, Transient Electromagnetic Fields Near a Cylindrical Antenna Multiply-Loaded with Lumped Resistors, August 1968.
3. Carl E. Baum, Sensor and Simulation Note 81, Resistively Loaded Radiating Dipole Based on a Transmission-Line Model for the Antenna, April 1969.
4. T. T. Wu and R. W. P. King, The Cylindrical Antenna with Nonreflecting Resistive Loading, IEEE Trans. on Antennas and Propagation, AP-13, May 1965, pp. 369-373.
5. L. C. Shen and R. W. P. King, The Cylindrical Antenna with Nonreflecting Resistive Loading, IEEE Trans. on Antennas and Propagation, AP-13, November 1965, p. 998.
6. AMS 55, Handbook of Mathematical Functions, National Bureau of Standards, 1964.